



# 1 Aerosol optical properties derived from POLDER- 2 3/PARASOL (2005-2013) over the western Mediterranean Sea 3 – Part 2 : Spatial distribution and temporal variability

4  
 5 Isabelle Chiapello<sup>1</sup>, Paola Formenti<sup>2</sup>, Lydie Mbemba Kabuiku<sup>2</sup>, Fabrice Ducos<sup>1</sup>, Didier  
 6 Tanré<sup>1</sup>, François Dulac<sup>3</sup>

7  
 8 <sup>1</sup>Univ. Lille, CNRS, UMR 8518 – LOA – Laboratoire d’Optique Atmosphérique, F-59000 Lille, France

9 <sup>2</sup>LISA, CNRS UMR 7583, Université Paris Est Créteil, Université de Paris, IPSL, Créteil, France

10 <sup>3</sup>LSCE/IPSL, CEA-CNRS-UVSQ, Université Paris-Saclay, Gif-sur-Yvette, France

11  
 12 *Correspondence to:* Isabelle Chiapello (isabelle.chiapello@univ-lille.fr)

13  
 14 **Abstract.** The Mediterranean atmosphere is impacted by a variety of natural and anthropogenic aerosols, which  
 15 exert a complex and variable pressure on the regional climate and air quality. In this study, we investigate aerosol  
 16 spatial distribution and temporal evolution over the western Mediterranean Sea (west of longitude 20°E) using the  
 17 full POLDER-3/PARASOL aerosol data record derived from the operational clear-sky ocean algorithm (collection  
 18 3) available from March 2005 to October 2013. This 8.5-yr satellite data set includes retrievals at 865 nm of the  
 19 total, fine, and coarse mode aerosol optical depth (AOD, AOD<sub>F</sub>, and AOD<sub>C</sub>, respectively), Angström exponent  
 20 (AE), and the spherical/non-spherical partition of the coarse-mode AOD (AOD<sub>CS</sub> and AOD<sub>CNS</sub>, respectively). In a  
 21 previous paper (Formenti et al., 2018), these POLDER-3-derived aerosol properties have been carefully validated  
 22 over the study region, based on coincident ground-based and airborne aerosol measurements. Here we analyze the  
 23 spatial distribution, the seasonal cycle and interannual variability of this ensemble of products in three latitude  
 24 bands (34-38°N, 38-42°N, and >42°N) and for three sites (Ersa, Barcelona, Lampedusa) distributed on the western  
 25 basin. Overall the POLDER-3 AOD spatial distribution exhibits a well-known south-to-north decreasing gradient,  
 26 and a seasonal cycle characterized by enhanced aerosol loads in spring and summer, both controlled by Saharan  
 27 dust. POLDER-3 retrievals of AE, AOD<sub>F</sub>, AOD<sub>C</sub>, and fine mode fraction (AOD<sub>F</sub>/AOD) highlight the influence of  
 28 coarse particles in the southern part of the region, off the north African coast, and higher relative contribution of  
 29 fine particles in the northern part, off the south European coast, with all year long persistent elevated loads over  
 30 the Adriatic Sea. Over the rest of the western Mediterranean Sea, POLDER-3 retrievals show a more homogeneous  
 31 spatial distribution of fine particles than that of coarse particles, even though climatological means of AOD<sub>F</sub>  
 32 highlight seasonal differences in the order of a factor 2 between the cleanest conditions occurring in the southern  
 33 part of the basin in winter and those most polluted observed in its northern part in Spring. The seasonal and spatial  
 34 variability of AOD<sub>CNS</sub> is close to that observed for AOD<sub>C</sub>, whereas POLDER-3 exhibit relatively low and weakly  
 35 variable levels of coarse spherical particles (AOD<sub>CS</sub> < 0.05). Over the whole 2005-2013 period, annual POLDER-  
 36 3 AOD evolution shows a decreasing trend (≥ 0.003 per year in absolute value). Such a decrease is much more  
 37 pronounced for AOD<sub>F</sub> (≥ 0.002 per year) than for AOD<sub>C</sub> (≤ 0.002 per year). Our analysis also suggests that the  
 38 North Atlantic Oscillation (NAO) index explains a significant part of the interannual variability of POLDER-3  
 39 AOD<sub>C</sub>, reflecting its role on the frequency of Saharan dust transport over the region. Finally, the POLDER-3  
 40 dataset highlights an improvement of air quality related to the fine aerosol component, with an evolution toward



41 more frequent occurrence of clean conditions ( $\geq 70\%$  of daily  $AOD_{F-865\text{ nm}} < 0.05$ ) at the end of the period of study  
 42 (2010-2013) over the western Mediterranean Sea.

## 43 44 **1 Introduction**

45 Due to the contributions of diverse natural and anthropogenic sources and because of their relatively short lifetime  
 46 in the troposphere, aerosols consist in a complex, timely and spatially variable mixture of particles (Boucher,  
 47 2015). As aerosol impacts, especially in terms of air quality degradation and radiative forcing contribution to  
 48 climate change, strongly depend on both very variable aerosol loads and properties, they require a dedicated  
 49 reliable monitoring. Despite a number of measurements efforts deployed in the last decades (Laj et al., 2009;  
 50 Pandolfi et al., 2018; Formenti, 2020; Laj et al., 2020), the variety of atmospheric particles, in terms of loads, size  
 51 ranges, shapes, chemical compositions, and optical properties remains partially characterized. Indeed, the  
 52 monitoring of the spatial, temporal, and vertical variability of all these physico-chemical parameters in both an  
 53 accurate and comprehensive way is still a challenge. Significant advances have been achieved by intensive field  
 54 experiments deploying detailed but limited in time and space *in situ* measurements of aerosol chemical, physical,  
 55 and optical properties (e.g. Denjean et al., 2016; Di Biagio et al., 2016). In parallel, remote sensing observations,  
 56 especially those from ground-based global aerosol networks, like AERONET (Holben et al., 2001), and dedicated  
 57 advanced aerosol satellite sensors, like MODIS (MODerate resolution Imaging Spectrometer) or POLDER  
 58 (POLarization and Directionality of the Earth's Reflectances) (Tanré et al., 2011; Bréon et al., 2011; Remer et al.,  
 59 2020), have made considerable progress in expanding in time and space the aerosol datasets acquired from field-  
 60 experiments. Thus, remote sensing has become an essential complementary tool, able to provide unique repetitive  
 61 and large-scale view of aerosol loads and properties evolution. The combination of both types of measurements,  
 62 i.e. detailed *in situ* aerosol characterization and long-term repetitive aerosol properties monitored by space-borne  
 63 sensors is required to improve current understanding of their evolution in terms of loads and properties and to  
 64 reduce uncertainties on their impacts.

65 This paper is dedicated to a regional aerosol analysis based on retrievals from POLDER-3/PARASOL  
 66 (Polarization & Anisotropy of Reflectances for Atmospheric Sciences coupled with Observations from a Lidar)  
 67 satellite sensor over the period 2005-2013 in the western Mediterranean Sea. This region, impacted by  
 68 demographic pressure and air quality degradation, is under the influence of both anthropogenic and natural  
 69 aerosols, emitted from different types of continental and marine sources (e.g. Lelieveld et al., 2002; Di Biagio et  
 70 al., 2015; Ancellet et al., 2016; Chazette et al., 2016, 2017; Claeyss et al., 2017; Michoud et al., 2017; Chazette et al.,  
 71 2019). Therefore, in the recent years, it has experienced an increasing scientific interest as shown by a number of  
 72 studies dedicated to Mediterranean aerosol characterization through large-scale field-experiments (e.g., Di Biagio  
 73 et al., 2015; Mallet et al., 2016; Ricaud et al., 2018 and references therein), modeling efforts (Rea et al., 2015;  
 74 Menut et al., 2016; Sič et al., 2016; Chrit et al., 2018; Drugé et al., 2019), and satellite observations analysis (Nabat  
 75 et al., 2013; Floutsi et al., 2016). Historical long-term aerosol satellite datasets have been used to investigate the  
 76 influence and evolution of north African mineral dust transported over this region (Dulac et al., 1992; Moulin et  
 77 al., 1998; Antoine and Nobileau 2006; Gkikas et al., 2013, 2016). Specific studies, often based on MODIS aerosol  
 78 retrievals or combining MODIS to other complementary aerosol satellite data sets, have attempted to separate the  
 79 contributions of different aerosol types prevailing in the Mediterranean region, i.e. maritime aerosols,  
 80 continental/anthropogenic aerosols, and African dust (Barnaba and Gobi, 2004; Hatzianastassiou et al., 2009;  
 81



Georgoulas et al., 2016). Despite the increasing number of satellite-based aerosol studies, especially in the East part of the Mediterranean area (Georgoulas et al., 2016; Shaheen et al., 2020), it is noticeable that no investigation of POLDER-3/PARASOL aerosol products (Herman et al., 2005; Tanré et al., 2011) has been performed yet over this region, despite its potential for monitoring the size-resolved aerosol properties over sea surfaces over its almost 9 years period of operation (Formenti et al., 2018).

In order to ensure a reliable regional view of aerosol loads and properties evolution from satellites, aerosol retrievals derived from different sensors and algorithms require careful evaluation. POLDER-3 aerosol retrievals validation has been performed for derived total and fine aerosol optical depth (AOD) through statistical comparison to sun/sky photometer data of the AERONET network at a global scale (Bréon et al., 2011). In a first dedicated paper (part 1 of the present paper: Formenti et al., 2018), we lead a regional comprehensive quality assessment of POLDER-3 derived aerosol parameters over the western Mediterranean Sea, based on both aerosol measurements from 17 ground-based coastal and insular AERONET sites over the period 2005-2013, and in situ airborne observations available during summer 2012 and 2013 Chemistry-Aerosol Mediterranean Experiment (ChArMEx) experiments (Di Biagio et al., 2015; Mallet et al., 2016). Our analysis has highlighted quality and robustness of POLDER-3 operational aerosol retrievals over oceans, especially total, fine, and coarse AOD (AOD, AOD<sub>F</sub>, and AOD<sub>C</sub>) at 865 nm, Angström Exponent (AE), and the spherical and non-spherical partition of coarse-mode AOD (AOD<sub>CS</sub> and AOD<sub>CNS</sub>) over this region.

In this paper, the advanced aerosol data set provided by POLDER-3 over its operating period, i.e. from March 2005 to October 2013, is investigated in terms of spatial variability and temporal evolution of aerosol load and properties over the western Mediterranean Sea.

## 2 POLDER-3 instrument and derived aerosol operational products over ocean

POLDER-3 (POLarization and Directionality of the Earth's Reflectances) instrument on board the PARASOL (Polarization & Anisotropy of Reflectances for Atmospheric Sciences coupled with Observations from a Lidar) mission is dedicated to advanced aerosol monitoring (Tanré et al., 2011). PARASOL, launched in December 2004 in order to be part of the A-Train, has been in operation from March 4, 2005 to October 10, 2013. Over this period, data availability is 91%. The explanations for the 9% loss of data are multiple: orbital maneuvers, instrument put on standby for security reasons, data transmission between the payload and the receiving station, and problems encountered with the stellar sensor. POLDER-3 payload consisted of a digital camera with a 274 x 242 –pixel CDD detector array, wide-field telecentric optics and a rotating filter wheel enabling measurements in 9 spectral channels from blue (443 nm) to near-infrared (1020 nm). Polarization measurements were performed at 490 nm, 670 nm, and 865 nm. With an acquisition of a sequence of images every 20 sec, the instrument could observe ground targets from up to 16 different angles,  $\pm 51^\circ$  along track and  $\pm 43^\circ$  across track (Tanré et al., 2011). The original pixel size is 5.3 km x 6.2 km at nadir. Algorithms have been developed to process the POLDER measurements in order to retrieve aerosol parameters at 18.5 x 18.5 km<sup>2</sup> superpixel resolution (3 x 3 pixels). In this paper, we use the operational clear-sky ocean retrieval algorithm (Herman et al., 2005) derived from collection 3, corresponding to the latest update performed in 2014 that included calibration improvements (Fougnie, 2016). This algorithm, described in details by Herman et al. (2005) and Tanré et al. (2011), has been slightly improved in collection 3 regarding non-spherical particles in the coarse mode (Formenti et al., 2018). Briefly, it is based on the total and polarized radiances measured at 670 and 865 nm. Using a look up table (LUT) built on aerosol



microphysical models (described in Table S1 in the Supplement of Formenti et al., 2018), the algorithm recalculates for each clear sky pixel the observed polarized radiances at several observational angles. Importantly, in the aerosol models used for the inversion, aerosols are considered as non-absorbing (the imaginary part of the refractive index is assumed as zero) and the real part of their refractive index is invariant between 670 and 865 nm. The aerosol number size distribution is lognormal and bimodal with an effective diameter smaller (larger) than 1.0  $\mu\text{m}$  for the fine (coarse) mode. The coarse mode includes a non-spherical fraction based on the spheroidal model from Dubovik et al. (2006), whereas a Mie model for homogeneous spherical particles is used to calculate multi-spectral and multi-angle polarized radiances. As an improvement compared to former versions of the algorithm, the effective diameter of the spheroidal model is allowed to take two values (namely 2.96 and 4.92  $\mu\text{m}$ ) in collection 3 (Table S1 of Formenti et al., 2018). Within the coarse mode, the non-spherical fraction is set to 5 discrete values (0.00, 0.25, 0.50, 0.75, and 1.00, Tanré et al. (2011)). A quality flag index (0 indicating the lowest and 1 the highest quality) is attributed to each superpixel depending on the inversion quality. As in Formenti et al. (2018), only POLDER-3 aerosol products derived from pixels with a quality flag  $\geq 0.5$  have been considered in our analysis. In the present study, we focus on the western Mediterranean region, west of longitude 20°E, considering the main aerosol parameters derived by POLDER-3 ocean operational algorithm: (i) available for all clear sky pixels: total, fine, and coarse aerosol optical depth (respectively AOD, AOD<sub>F</sub>, and AOD<sub>C</sub>) at 865 nm, and Angström Exponent between 670 and 865 nm (AE), (ii) available only when the geometrical conditions are optimal (scattering angle range of roughly 90°-160°): spherical and non-spherical fractions of the AOD in the coarse mode ( $f_{CS}$  and  $f_{CNS}$  respectively), allowing to assess AOD<sub>CS</sub> and AOD<sub>CNS</sub> (spherical and non-spherical coarse AOD, respectively) at 865 nm. The quality of these POLDER-3 derived aerosol parameters has been evaluated over the region of interest by Formenti et al. (2018), using co-located in situ airborne measurements from summer 2012 and 2013 field-experiments and coincident ground-based AERONET data available from 17 insular and coastal sites over the whole POLDER-3 operation period (2005-2013). This first comprehensive regional evaluation has provided new assessments of uncertainties and highlighted the good quality of collection 3 POLDER-3 aerosol data set over our area of interest (Table 4 of Formenti et al., 2018). In our regional analysis of spatial distribution and temporal variability of POLDER-3 aerosol retrievals, the AOD, AOD<sub>F</sub>, and AOD<sub>C</sub> derived at 865 nm will be complemented, through an extrapolation with the Angström Exponent, by those at 550 nm, which is the standard wavelength of many aerosol satellite retrievals and model simulations (Nabat et al., 2013).

## 3 Results

### 3.1 Mean regional and seasonal picture (2005-2013)

The climatological (March 2005 – October 2013) seasonal maps of POLDER-3 derived AOD, AE, AOD<sub>F</sub>, AOD<sub>C</sub>, AOD<sub>F</sub>/AOD (i.e. Fine Mode Fraction or FMF), AOD<sub>CNS</sub>, and AOD<sub>CS</sub> at 865 nm over marine areas in the region 30-50°N, 10°W-20°E, i.e. mainly the western Mediterranean Sea, are shown in Figure 1. The total AOD (left panels) exhibits a pronounced seasonality with minimum values in winter (defined by the December-January-February months): AOD < 0.10 over most of the region of study. In spring (March-April-May), AOD shows an increase, especially intense over the southeastern part of the region between Italy and Africa, whereas the maximum AOD values ( $\geq 0.20$ ) are reached in summer (June-July-August) over the whole southern part of the area. In autumn (September-October-November), the AOD over the region are mostly low, comparable to winter



loads, except over the southeastern part of the domain, especially over the Ionian Sea, and off the coast of Tunisia, Lybia and south of Sicily, where they reach moderate values (range 0.10 – 0.15). This area of enhanced aerosol transport is geographically similar to that associated to maximum AOD (~ 0.20) in spring. In general, the seasonal POLDER-3 total AOD maps exhibit a well-established south-to-north gradient, with a decrease of values toward the northern part, reflecting the high influence of aerosol sources from the North African continent. This aerosol spatial distribution is consistent with that derived by other satellite sensors over the Mediterranean basin (for example Moulin et al., 1998, Barnaba and Gobi, 2004; Papadimas et al., 2008). The  $AE_{865-670\text{ nm}}$  seasonal maps (second column panels) highlight the influence of coarse aerosols (associated with low AE values) in the south part of the region off the north African coast, and higher contribution of fine particles along the coasts of Europe, especially over the Adriatic Sea, where AE values are equal or higher than 1, in all seasons.  $AOD_F$ ,  $AOD_C$ , and  $AOD_F/AOD$  (FMF) seasonal maps, shown in the three central column panels, confirm this pattern of spatial variability, typical of coarse and fine aerosol repartition in the Mediterranean basin. The seasonal and spatial variability of  $AOD_{CNS}$  is close to that observed for  $AOD_C$ , whereas POLDER-3 retrievals of  $AOD_{CS}$  suggest a relatively homogeneous repartition of coarse spherical particles, with low values ( $AOD_{CS} < 0.05$ ), and no substantial spatial and seasonal variations (right panels of Figure 1). Figure S1 of the supplementary material complements these POLDER-3 seasonal maps at 865 nm, with  $AOD$ ,  $AOD_F$ ,  $AOD_C$ , and  $AOD_F/AOD$  (i.e. FMF) extrapolated at 550 nm. At this wavelength, AOD reach higher values ( $\geq 0.30$  during summer maximum),  $AOD_F$  are strongly enhanced (values up to 0.16-0.20) compared to 865 nm ( $< 0.08$ ), whereas  $AOD_C$  values are only slightly modified. These ranges of values are consistent with the stronger wavelength dependence of AOD of small particles, characterized by high AE values, inducing pronounced increase of  $AOD_F$  values toward shorter wavelengths. Thus, the spatial distribution of POLDER-3  $AOD_F$  at 550 nm is characterized by maximum values ( $> 0.10$ ) over the eastern part of the region of study, and seasonal peaks in spring and summer. North of the Adriatic Sea, POLDER-3 highlights an area characterized by all-year persistent high values of  $AOD_F$  ( $> 0.12$  at 550 nm), most probably reflecting accumulation of pollution particles due to influence of regional anthropogenic sources (as for example from Northern Italy in the Po Valley).

### 3.2 Sub-regional features

In order to examine more deeply the seasonal variations of POLDER-3 aerosol retrievals accounting for the south-to-north gradient observed in Figure 1, the area of study has been divided into three main latitudinal sub-regions. These regions are illustrated in Figure 2. They correspond respectively to the northern part (north of latitude  $42^\circ\text{N}$ : zone 1 called NW MED), the central part (latitude band  $38 - 42^\circ\text{N}$ , zone 2 called CW MED), and the southern part (south of latitude  $38^\circ\text{N}$ : zone 3 called SW MED) of the western Mediterranean Sea ( $6^\circ\text{W} - 20^\circ\text{E}$ ).

Figure S2 of the supplementary material reports the statistics of the POLDER-3 retrievals over the March 2005-October 2013 time period in each-sub-region, with mean and standard deviations, maximum and minimum values of number of available clear-sky superpixels (left column) and number of available days of observations for each month and year (right column). The maximum number of POLDER-3 superpixels (left panels) is 434 in NW MED and up to 1232 in SW MED and 1384 in CW MED, reflecting the smaller size of the NW-MED sub-region. As expected, more POLDER-3 retrievals are available in summer than in winter months, due to the higher influence of cloudiness during the cold season. The number of days with aerosol retrievals by month and year for each sub-region (right column) highlights that more than 50% of daily POLDER-3 retrievals are available for most of the



months of the whole time period. A few exceptions occur for some specific months, as July 2007 and July 2010, common at the three sub-regions due to missing data during these periods related to instrumental problems with the solar sensor (only 28% and 14% of data available, respectively). A reduced number of days of POLDER-3 aerosol retrievals is observed in the NW MED sub-region in November and December 2012 (respectively 11 and 4 days, Figure S2b), likely due to an unfavorable combination of cloudiness and spatial coverage in the northernmost part of our study region during these two months. Beyond this particular case, this analysis generally suggests that the cloudiness significantly reduces the number of POLDER-3 pixels available over each sub-region from October to March (Figure S2a,c,e), even though the number of available days of POLDER-3 observations remains reasonable (Figure S2b,d,f).

Figure 3 illustrates the 8- or 9-year climatological mean over March 2005 – October 2013 of monthly POLDER-3 derived aerosol parameters at 865 nm over the three sub-regions defined in Figure 2. The averaged seasonal cycle of AOD is relatively similar over the north and central parts of the basin, whereas the southern part shows generally higher total aerosol loads, and a more pronounced seasonal variability, with two maxima in April-May and July (mean  $AOD_{865\text{ nm}} > 0.15$ ). The mean monthly variations of the POLDER-3  $AOD_F$  integrated over the three sub-regions are remarkably similar, in agreement with previous analysis based on ground-based AERONET observations suggesting that the aerosol fine mode is, to some extent, relatively homogeneously distributed over the western Mediterranean region (Lyamani et al., 2015; Sicard et al., 2016). Conversely, the north-south gradient clearly appears for  $AOD_C$  (right column middle panel of Figure 3), especially for the SW MED area, consistently with what is observed for total AOD. The seasonal variations of the monthly-averaged AE (left column middle panel) reflect the north-south gradient of aerosol sizes, with an increased influence of smaller particles toward the north, a pattern confirmed by the monthly evolution of FMF (left column, bottom panel). The monthly-averaged  $AOD_{CS}$  (right column, bottom panel) shows very low seasonal and spatial variability, as previously observed in Figure 1, whereas the POLDER-3 mean  $AOD_{CNS}$  seasonal cycle illustrates much more pronounced monthly and north-south evolution, in coherence with those of  $AOD_C$  and total AOD. Figure S3 in the supplementary material illustrates the climatological mean of monthly POLDER-3 AOD,  $AOD_F$ ,  $AOD_C$ , and FMF extrapolated at 550 nm, confirming the patterns displayed Figure 1, especially the marked increase of  $AOD_F$  values, and FMF at this wavelength.

The POLDER-3 mean seasonal aerosol retrievals displayed in Figure 1 and 3 at 865 nm are summarized in Table 1a, those extrapolated at 550 nm (Figures S1 and S3) in Table 1b. The multi-annual averages of AOD,  $AOD_C$  and  $AOD_{CNS}$  at 865 nm in Table 1a confirm the north-south gradient with minimum values in the north part (0.090, 0.055, and 0.043 respectively for AOD,  $AOD_C$ , and  $AOD_{CNS}$ ) compared to the south part of the western Mediterranean basin (0.124, 0.091, 0.073 respectively). POLDER-3 AE and FMF mean multi-annual values consistently highlight an increase in the coarse component of AOD toward the south. In terms of multi-annual averages, the  $AOD_F$  remains relatively uniform, with some minor variations indicating minimum fine mode aerosol loads in the central area (0.032 in CW MED), maximum in the north (0.035 in NW MED) and intermediate values in the south part (0.033 in SW MED), these variations being more pronounced at 550 nm (Table 1b). Seasonal multi-annual averages of  $AOD_F$  highlight differences in the order of a factor 2 between minimum values in the south in winter (around 0.02 at 865 nm, 0.06 at 550 nm) and maxima in spring (around 0.04 at 865 nm, and 0.12 at 550 nm), especially in the northern part of the region. The POLDER-3 derived mean multi-annual  $AOD_{CS}$





at 865 nm (Table 1a) reveal some seasonal variability, with maximum values in summer in the south part (0.031) and minimum in winter in the northern part (0.013). Although reasons for such an evolution are not fully understood, considering the similarity with that of  $AOD_{CNS}$ , this variability could be partly related to the influence of North African dust transport rather than fully representative of a background coarse sea-salt fraction (Claeys et al., 2017). Indeed, Saharan dust might include a spherical coarse aerosol fraction following mixing with soluble secondary components such as sulfate and nitrate (Drugé et al., 2019).

### 3.3 Temporal evolution at selected sites

The previous regional analysis is complemented by the investigation of the POLDER-3 aerosol properties around three contrasted AERONET sites of the western basin: Ersu (43.00367°N, 9.35929°E, altitude 80 m), the northernmost site located on northern coast of Corsica Island, France; Lampedusa (35.51667°N, 12.63167°E, alt. 45 m) the southernmost site located on the northwestern coast of Lampedusa Island, Italy; Barcelona (41.38925°N, 2.11206°E, alt. 125 m) the westernmost site located in a urban/coastal environment on the shore of northeastern Spain (Figure 2). Ersu and Barcelona are sites under the influence of long-range Saharan dust transport, whereas Lampedusa is subject to short to medium-range dust transport. Ersu and Lampedusa are marine background sites with some anthropogenic influence, Barcelona is located in a heavily polluted environment. Ersu and Lampedusa were the two super-sites of the ChArMEx (The Chemistry-Aerosol Mediterranean Experiment) collaborative research program, and Barcelona, which is also part of EARLINET/ACTRIS network, one of the secondary sites of this program (Mallet et al., 2016). In this context, many experimental set up of in situ aerosol measurements provided detailed aerosol characterization. Additionally, the long-term AERONET routine aerosol measurements at these sites have been used for the comprehensive regional validation of POLDER-3 retrievals presented in Formenti et al. (2018). Here we considered the same POLDER-3 dataset, by selecting superpixels within  $\pm 0.5^\circ$  around the AERONET sites, corresponding to a maximum number of 17 at Ersu, 28 at Lampedusa, and 13 at Barcelona.

#### 3.3.1 Monthly time series

Figure 4 illustrates the month-to-month evolution from March 2005 to October 2013 of POLDER-3 retrievals at 865 nm, extracted at Ersu, including (a) AOD, (b)  $AOD_F$  and  $AOD_C$ , (c)  $AOD_{CNS}$  and  $AOD_{CS}$ , (d)  $AE_{865-670}$  and FMF. The total aerosol load derived from POLDER-3 at this site show a marked variability, both at seasonal and interannual time scales, with a maximum recorded value of monthly averaged AOD of 0.21 (June 2007), and winter minimum values of AOD around 0.05. Monthly-averaged AOD values above 0.10 occur mostly during spring (April-May) and summer (June-July) seasons. Interestingly, Figure 4a highlights some additional peak of AOD occurring in autumn for specific years, as for example in September-October 2008. Month-to-month evolution of AE and FMF reported on Figure 4d show remarkably similar variability, which confirms that the AE is a good proxy of the proportion of fine particles component relative to total AOD. The average monthly FMF of the AOD at 865 nm at Ersu is estimated at 37% by POLDER-3 in all clear-sky conditions, with a range of monthly mean values between 18% and 65%, and only 17 months over 103 (i.e. 17%) with FMF greater or equal to 50% (considering 865 nm wavelength). These occurrences are mostly recorded in late winter (February-March) and autumn (September-October-November) and are generally characterized by moderate monthly mean AOD values (between 0.06 and 0.13). Figure 4b illustrates the month-to-month evolution of  $AOD_F$  and  $AOD_C$ , confirming that



at this wavelength (865 nm), the AOD is mostly dominated by the coarse mode fraction (63% on average). For some specific months of the time series, as for example September 2005, July 2006, September 2009, February/March 2010, the POLDER-3 derived  $AOD_F$  is higher than  $AOD_C$ , but these cases are rather rarely observed in comparison to those corresponding to the dominance of the AOD coarse mode component. The monthly evolution of POLDER-3  $AOD_{CS}$  and  $AOD_{CNS}$  at Ersa, reported in Figure 4c also suggests a strong domination of non-spherical particles in the coarse mode AOD over most of the 8.5-year time series. A few cases with  $AOD_{CS}$  greater or equal to  $AOD_{CNS}$  did occur over the period, as for example in August 2010, June 2011, or July 2012. They need to be explored, although they clearly do not reflect the most frequent aerosol conditions in Ersa. Considering only the POLDER-3 retrievals available in Best Viewing Conditions, the averaged repartition in terms of aerosol size mode and shape contributions to the total AOD at 865 nm at Ersa are 36% for the fine AOD, 44% for the non-spherical coarse mode and 20% for the spherical coarse mode. These estimates are consistent with the POLDER-3 data set available in all clear sky conditions, which estimate 63% of coarse mode AOD versus 37% of fine mode AOD at 865 nm.

Similarly to Figure 4, Figure 5 and 6 illustrate the month-to-month evolution from March 2005 to October 2013 of POLDER-3 retrievals at 865 nm, extracted at Barcelona and Lampedusa respectively, including (a) AOD, (b)  $AOD_F$  and  $AOD_C$ , (c)  $AOD_{CNS}$  and  $AOD_{CS}$ , (d)  $AE_{865-670}$  and FMF. Consistently with the influence of short to medium range Saharan dust transport expected in Lampedusa, POLDER-3 AOD show their highest monthly mean values at this site (up to 0.44 in May 2011, Figure 6a), compared to both Ersa (max of 0.21 in June 2007, Figure 4a) and Barcelona (max of 0.24 in June 2006, Figure 5a). These maximum AOD values are clearly associated to coincident maximum values of monthly mean  $AOD_C$ , with 0.39 in May 2011 in Lampedusa (Figure 6b), 0.18 in June 2006 in Barcelona (Figure 5b), and 0.16 in June 2007 in Ersa (Figure 4b). Figure 4-6 clearly highlight that POLDER-3 monthly mean AOD values above 0.10 are much more frequent in Lampedusa (66% of frequency over the 104 months of POLDER-3 observations) than in Barcelona (43% of frequency) and Ersa (30%). The contrast between the three sites is even more pronounced considering the  $AOD_C$  retrievals, as the frequency of monthly values above 0.10 (44%, 22%, and 5% for Lampedusa, Barcelona, and Ersa, respectively) clearly highlights the more frequent impact of coarse particles, especially non-spherical desert dust, in Lampedusa. Conversely, the monthly evolution of  $AOD_F$  reported in Figure 4b, 5b, and 6b does not show such a marked contrast, nor with respect to the maximum values, rather comparable at the three sites (0.072, 0.074, and 0.076 in Ersa, Barcelona, and Lampedusa, respectively), or the frequency of monthly mean values above 0.04 (27%, 31% and 34% respectively). At Lampedusa, monthly  $AOD_F$  are always substantially lower than monthly  $AOD_C$  (Figure 6b). At Barcelona monthly  $AOD_F$  are mostly below  $AOD_C$  (Figure 5b), with the noticeable exception of a few months over the time period, generally in winter or late summer (Feb. 2006, Feb. 2008, Sept. 2009 for example), characterized by the dominance of  $AOD_F$ . These months with POLDER-3 mean derived FMF greater than 50% represent a frequency of 10% over the whole monthly data set in Barcelona (Figure 5d), and 0% in Lampedusa (Figure 6d). Compared to their frequency in Ersa (17%, Figure 4d), POLDER-3 retrievals of fine and coarse components of AOD suggest that the influence of fine particles is more frequent in Ersa, possibly due to the transport of polluted air masses from highly industrialized regions (Po Valley, Marseille-Fos-Berre for example) in the north part of the basin (Mallet et al., 2016). These features may also simply reflect the more frequent influence of desert dust at Lampedusa and in a less extent at Barcelona, which may hide the possible influence of fine aerosols of anthropogenic origin at these two sites. Over the whole POLDER-3 observing period, maximum





monthly mean values of AOD<sub>CS</sub> range from 0.058 in Ersa (March 2008, Figure 4c) to 0.075 in Lampedusa (April 2008, Figure 6c) and 0.090 in Barcelona (November 2009, Figure 5c). Frequencies of monthly mean POLDER-3 AOD<sub>CS</sub> values above 0.03 are 13%, 31%, and 38% at Ersa, Barcelona, and Lampedusa respectively. Such a variability suggests some impact of desert dust on AOD<sub>CS</sub>, although the contribution of sea-salt particles or a combination of both aerosol types cannot be excluded without further investigations. Maximum monthly AOD<sub>CNS</sub> values range from 0.109 at Ersa (Sept. 2008 and May 2009, Figure 4c) to 0.210 at Barcelona (Nov. 2009, Figure 5b) and 0.220 at Lampedusa (March 2005, Figure 6b). Frequencies of monthly mean POLDER-3 AOD<sub>CNS</sub> values above 0.03 reach 91% in Lampedusa, 70% in Barcelona, and 67% in Ersa. Considering only the POLDER-3 retrievals available in Best Viewing Conditions, the averaged contributions in terms of aerosol size and shapes at Barcelona are rather similar to those estimated at Ersa, with 34% of fine AOD, 46% of coarse non-spherical AOD and 20% of coarse spherical AOD at 865 nm. At Lampedusa, the averaged contribution of fine AOD is reduced to 26%, with a higher contribution of coarse non-spherical AOD (55%), and a rather constant relative contribution of coarse spherical AOD (19%).

### 3.3.2 Daily time series

Figure 7 shows the daily evolution from March 4, 2005 to October 10, 2013 of POLDER-3 AOD (a), AOD<sub>F</sub>(b), AOD<sub>C</sub>(c), AOD<sub>CS</sub>, and AOD<sub>CNS</sub> (d) at 865 nm at Ersa, Barcelona, and Lampedusa. Table 2 presents a statistical summary of the daily POLDER-3 aerosol retrievals for these three sites. The range of AOD values varies from 0.01 to 0.68 at Ersa, 0.01 to 1.05 at Barcelona, and 0.02 to 4.72 at Lampedusa, indicating the occurrence of extreme AOD events at the southernmost site of Lampedusa. Daily AOD > 0.3 occur 9% of the time in Lampedusa. For these days, POLDER-3 retrieves low AE (0.41 in average), low FMF (21% in average), and high contribution of non-spherical aerosol fraction in the coarse mode (87% in average), consistently with the dominant influence of desert dust. Such an influence is verified at Barcelona as well: although much less frequent (less than 3% of occurrence), daily AOD > 0.3 are associated to average AE values of 0.44, average FMF of 21% (maximum 45%) and average non-spherical aerosol fraction in the coarse mode of 85%. Finally, at Ersa POLDER-3 retrievals of daily AOD > 0.3 are rare (< 2% of occurrence over the POLDER-3 observing period), and characterized by the same properties typical of desert dust influence (mean AE 0.31, mean FMF 16%, mean non-spherical aerosol fraction in the coarse mode of 71%). These POLDER-3 retrievals are consistent with the Gkikas et al. (2013) climatology of intense desert dust events in the Mediterranean, which recorded extreme dust episodes mostly in the southern part of central Mediterranean, where Lampedusa is located. These authors also reported that these extreme desert dust episodes are characterized by AOD<sub>550nm</sub> values > 2.5 and up to 4. At Lampedusa, Figure 7b and 7c suggest that the most intense AOD peaks are always associated to an increase in AOD<sub>C</sub>, and in some cases in AOD<sub>F</sub> as well. Thus, for the three main sites considered here, the aerosol retrievals recorded by POLDER-3 from 2005 to 2013 highlight the high variability of both the total and the size- and shape-segregated components of the AOD. The background aerosol conditions, corresponding to low POLDER-3 AOD<sub>865 nm</sub> (< 0.05) show an average occurrence of 22% of the time in Ersa, 20% in Barcelona and only 9.5% in Lampedusa. These features show that, over the March 2005 – October 2013, POLDER-3 has recorded very low occurrence of pristine days, i.e. clean conditions associated to low aerosol loads, especially at Lampedusa. As reported in Table 2, the average daily AOD (865 nm) is 0.09 (standard deviation 0.07) in Ersa, 0.10 (standard deviation 0.04) in Barcelona, and 0.15 (standard deviation 0.18) in Lampedusa, reflecting both higher frequency and intensity of aerosol episodes in Lampedusa, as illustrated in Figure 7a. This main pattern is also verified for POLDER-3 retrievals of AOD<sub>C</sub> and



to a certain extent  $AOD_F$ , which reach their maximum values in Lampedusa (4.4 and 0.35, respectively). However, POLDER-3 shows that at 865 nm, the  $AOD_F$  is always lower than 0.2 (Figure 7b), except at Lampedusa for a reduced number of days (4). At this site, peaks of  $AOD_F$  seem to be associated to peaks of  $AOD_C$ , suggesting the influence of desert dust on both aerosol size components, and/or the double influence of two different aerosol types (i.e., possibly both dust and anthropogenic). POLDER-3  $AOD_{CS}$  and  $AOD_{CNS}$  time series, shown Figure 7d, are more difficult to interpret, first of all because the sampling is reduced by more than 50% compared to POLDER-3 retrievals associated to all clear sky pixels (ACSP, i.e.,  $AOD$ ,  $AOD_F$ ,  $AOD_C$ ,  $AE$ ), due to the necessity of best viewing conditions (BVC) for their retrieval, as reported in Table 2. Despite this limitation, Figure 7d and Table 2 show high variability of both spherical and non-spherical aerosols in the coarse mode, with a larger range of daily values for  $AOD_{CNS}$  (up to 1.00 in Lampedusa) than for  $AOD_{CS}$  (maximum 0.34 in Barcelona). At the three sites considered here, POLDER-3 mean retrievals of daily  $AOD_{CNS}$  (0.04 – 0.08) are on average more than two times larger than those of  $AOD_{CS}$  (0.02 – 0.03).

### 3.4 Inter-annual evolution

Annual maps of POLDER-3  $AOD$ ,  $AOD_C$ , and  $AOD_F$  at 865 nm are displayed for each of the 9 available observations years (2005 to 2013) in Figure 8. The annual averages are computed over the period March–October only in order to consistently consider the 9 years in the whole available period. The left period November–February is hopefully the period where  $AOD$  is the lowest in the region (Figure 3). Figure 8 highlights a significant interannual variation in  $AOD$  (left column), characterized by elevated aerosol loads for specific years, as 2007 and 2008, and lower  $AOD$  ranges in 2009 and 2013. The interannual variations of POLDER-3  $AOD_C$  (middle column) tend to be relatively similar to those of  $AOD$ , especially over the south part of the basin. Figure 8 also suggests that the maximum values of  $AOD_F$  (right column) were observed in the first half of the period of study, with an evolution toward more moderate to low loads in fine particles apparent from 2010. Figure S4 of the supplementary material confirms such an evolution with annual maps of POLDER-3  $AOD_F$  extrapolated at 550 nm for each of the 9 observation years. The year 2007 appears highly polluted in fine particles over the whole basin. Over the most eastern part of the region, the intense plume observed by POLDER-3 can be related to the occurrence of devastating fires in Greece in the summer of 2007, producing large amounts of biomass burning aerosols transported downwind over the central Mediterranean (Kaskaoutis et al., 2011).

In order to analyze further these interannual evolutions, Figure 9 presents the time series of annual averages (left column) and monthly anomalies (right column) of POLDER-3  $AOD$ ,  $AOD_F$ , and  $AOD_C$  at 865 nm spatially averaged over the north, central, and south parts of the western Mediterranean basins (defined in Figure 2) for the period March 2005 – October 2013. The monthly anomalies are computed by subtracting to each monthly averaged value of a specific year its corresponding long-term monthly average (2005–2013). Linear regressions are applied to both March–October annual averages and monthly anomalies of POLDER-3  $AOD$ ,  $AOD_F$ , and  $AOD_C$  evolution as a function of time. The values of the slopes, reported in Table 3 provide the sign and magnitude of the trends at 865 nm. Slopes derived from the same analysis of POLDER-3  $AOD$ ,  $AOD_F$ , and  $AOD_C$  extrapolated at 550 nm are reported in Table S1 of supplementary material. The same approach is applied to POLDER-3  $AOD$ ,  $AOD_F$ , and  $AOD_C$  retrievals extracted at Ersa, Barcelona, and Lampedusa. Results are presented Figure 10, with trends and their statistical level of confidence reported in Table 4 at 865 nm (Table S2 of supplementary material at 550 nm). Overall, this analysis clearly reveals negative values of the trends for all the sub-regions and sites considered



over our study region, highlighting that POLDER-3 has recorded a general decrease of aerosol loads over western Mediterranean Sea over the period 2005–2013. The decreasing trends recorded for AOD interannual evolution are found to be statistically significant, at least at the 95% confidence level, over the northern and central part of the study region and, consistently, at Ersa and Barcelona (top panels of Figure 9 and 10). In contrast, for the southernmost part of the region (SW MED), the 95% confidence level is not reached when considering annual means of AOD and when AOD are extracted at Lampedusa (both from annual means and monthly anomalies), suggesting more uncertainties on the robustness of the decreasing trend. AOD<sub>c</sub> interannual evolutions recorded by POLDER-3 show decreasing trends, although the confidence level of 95% is only reached when considering monthly anomalies at Barcelona and for the three sub-regions (middle panels of Figure 9 and 10). The absolute values of the POLDER-3 AOD<sub>c</sub> decreasing trends, especially in the northern part of the basin (NW MED, trend  $\leq -0.0012 \text{ yr}^{-1}$ ) suggest a moderate-to-low decreasing tendency, around  $-0.01$  per decade. Interestingly, POLDER-3 AOD<sub>F</sub> interannual evolutions for the three sub-regions (bottom panels of Figure 9) clearly reveal robust decreasing trends, statistically significant at 99% level (Student's test). As reported in Table 3, considering the northern and central parts of the study region, AOD<sub>F</sub> decreased by  $-0.0020 \text{ yr}^{-1}$  at 865 nm ( $-0.005 \text{ yr}^{-1}$  at 550 nm, Table S1) whereas the decrease found in the southern part is slightly lower,  $-0.0016 \text{ yr}^{-1}$  at 865 nm ( $\leq -0.004 \text{ yr}^{-1}$  at 550 nm, Table S1). Analysis of POLDER-3 AOD<sub>F</sub> interannual variability at Ersa, Barcelona, and Lampedusa confirm these downward evolutions, with decreasing trends statistically significant at the 99% confidence level (Table 4 and bottom panels of Figure 10). The decrease trends seem to be more pronounced in Barcelona (between  $-0.0026 \text{ yr}^{-1}$  for annual means and  $-0.0029 \text{ yr}^{-1}$  for monthly anomalies, respectively) than in Lampedusa (between  $-0.0015 \text{ yr}^{-1}$  and  $-0.0017 \text{ yr}^{-1}$ ), with intermediate magnitudes at Ersa (between  $-0.0019$  and  $-0.0024 \text{ yr}^{-1}$ ). Consistently, the decreasing trends derived from POLDER-3 AOD<sub>F</sub> extrapolated at 550 nm vary between values around  $-0.007 \text{ yr}^{-1}$  at Barcelona,  $-0.005/ -0.006 \text{ yr}^{-1}$  in Ersa, and  $-0.004 \text{ yr}^{-1}$  in Lampedusa (Table S2).

The year-to-year variations in the North Atlantic Oscillation (NAO) have been examined in several past studies to support interpretation of inter-annual changes of north African dust transport either recorded by different satellite sensors, especially over the Mediterranean in the 1990s and early 2000s decades (Moulin et al., 1997; Antoine et Nobileau, 2006) or simulated by regional models (Nabat et al, 2020). In the present paper, we investigate the relationship between winter (December through March) NAO index defined by Hurrell (1995) and interannual variations of POLDER-3 AOD, AOD<sub>F</sub>, and AOD<sub>c</sub> from 2005 to 2013 over the three western Mediterranean sub-regions and sites considered in this work. The winter NAO indexes for the 2005–2013 period were obtained from "The Climate Data Guide: Hurrell North Atlantic Oscillation (NAO) Index (station-based)" (<https://climatedataguide.ucar.edu/climate-data/hurrell-north-atlantic-oscillation-nao-index-station-based>). The annual means of POLDER-3 AOD and AOD<sub>F</sub> do not show any statistically significant correlation with the winter NAO Index, although the correlation coefficients for annual AOD reach 0.51 at Ersa, and 0.66 for CW MED. The annual averages of AOD<sub>c</sub> confirm a link with the NAO for the CW MED region ( $r=0.70$ , with 95% confidence level). At Ersa, we obtain  $r=0.54$  which is not significant. These correlation levels, not observed in the southern areas of our study region (Lampedusa or SW MED), strongly suggest that the NAO exerts a control on north African dust transport rather than on their emissions over source-regions. In order to go further, we examine the relative frequency of desert dust episodes ( $f_D$ ) by selecting the days associated with POLDER-3 AOD<sub>c</sub> 865 nm  $\geq 0.10$  for the three-sub regions considered in our study. Figure 11 reports the results for the period 2005–2013 (March–October) along with the time series of the winter NAO Index. A significant correlation is confirmed



451 between NAO Index and  $f_D$  for the central part of the western Mediterranean region (blue curve,  $R=0.76$ , with  
 452 95% confidence level) and to a lesser extent for the northern part of the western Mediterranean region (green  
 453 curve,  $R=0.65$ , not significant). For the southern part of the region, the correlation is much lower ( $r=0.43$ ) although  
 454 some connection with NAO is apparent at the beginning of the period (2005–2009), the correlation being strongly  
 455 degraded by the opposition observed in 2010 between extremely low NAO index ( $-4.64$ ) and a relatively high  $f_D$   
 456 value (36%). It is noticeable that Salvador et al. (2014), in their analysis of interannual variations of African dust  
 457 outbreaks for years 2001–2011 over the western Mediterranean basin, excluded the year 2010 from their  
 458 correlation plots with NAO indexes considering that it was associated to an atypical low value of the NAO index,  
 459 most probably governed by anomalous atmospheric patterns. Interestingly, SW MED is the only of our three  
 460 regions where POLDER-3 has recorded a significant decreasing trend in  $f_D$  of  $-2\%$  ( $\pm 1\%$ ) per year over the period  
 461 2005–2013 ( $R=0.68$ , with 95% confident level).

462 We also consider the relative frequency of occurrence of clean conditions associated to low aerosol loads recorded  
 463 by POLDER-3 at 865 nm for the fine fraction (daily  $AOD_F < 0.05$ , top panels), the coarse fraction (daily  $AOD_C <$   
 464  $0.05$ , middle panels) and the total aerosol (daily  $AOD \leq 0.10$ , bottom panels), named  $f_{CF}$  (Clean Fine),  $f_{CC}$  (Clean  
 465 Coarse), and  $f_{CT}$  (Clean Total), respectively. Figure 12 reports the year-to-year evolutions of  $f_{CF}$ ,  $f_{CC}$ , and  $f_{CT}$  for the  
 466 three sub-regions, NW MED, CW MED, SW MED (left column) and Ers, Barcelona, Lampedusa (right column).  
 467 Clearly, POLDER-3 record an increasing trend in the frequency of occurrence of clean conditions for the fine  
 468 fraction of AOD, both for the three sub-regions and three sites. The  $f_{CF}$  trends vary between  $+2\%$  per year (SW  
 469 MED and Lampedusa),  $+3\%$  per year (CW MED, NW MED, Ers) and  $+4\%$  per year (Barcelona), with confidence  
 470 levels of 99% (except for SW MED where only 95% confidence level is reached). In Barcelona, the increase is  
 471 spectacular with clean conditions in fine particles occurring less than 60% of the time between 2005 and 2007  
 472 (minimum in 2007, with 51% of frequency) and reaching values above 75% in the 2011–2013 years (maximum in  
 473 2013, with 85% of frequency). Such an evolution is consistent with decreasing trends in surface  $PM_{2.5}$  at  
 474 background sites in Spain and Europe reported in the literature over 2002–2010 (Cusack et al., 2012). Pandolfi et  
 475 al. (2016) further observed decreasing trends between 2004 and 2014 in northeastern Spain, both at the background  
 476 site of Barcelona and at the regional background site of Montseny, and mostly related them to decreases in  
 477 industrial emissions and in secondary sulfate and nitrate fine particle concentrations. Regarding the coarse fraction  
 478 of AOD,  $f_{CC}$  records some significant year-to-year variability but no tendency, except for the SW MED sub-region  
 479 where a low, slightly positive trend ( $< +1\%$  per year, not significant) is recorded over the period 2005–2013,  
 480 suggesting a possible slow evolution toward cleaner conditions for the coarse aerosol fraction in the southern part  
 481 of the basin. Considering the total aerosol loads (bottom panels of Figure 12),  $f_{CT}$  evolution shows an increasing  
 482 trend (between  $+2$  and  $+3\%$  per year with a 95% confidence level) for the three sub-regions and three sites  
 483 considered.

484 Figure 13 and Figure 14 compare the 2005–2013 (March - October) mean values of  $AOD_F$  and  $AOD_C$  respectively  
 485 with their anomalies for each year of the period. The year-to-year evolution of  $AOD_F$  is clearly characterized by  
 486 positive anomalies in the first years of the period of study (especially, 2005–2007), and negative anomalies for the  
 487 most recent years. The spatial distribution of these anomalies indicate lower than long term means  $AOD_F$  over the  
 488 eastern part of the region in 2012, and mostly over the northern and western part of the region in 2013. Annual  
 489 anomalies of  $AOD_C$  illustrated in Figure 14 highlight elevated loads of coarse aerosols for specific years and areas  
 490 of the region, as in 2008 in the southeastern part or in 2012 in the western part of the basin. In contrast, 2009



(southeastern part), 2010 (western part), and 2013 (most of the basin) appear to be associated with lower than long-term means values of AOD<sub>c</sub>. These POLDER-3 interannual evolutions tend to confirm the association between increased dust transport during positive NAO phases (+2.1 in 2008, +3.17 in 2012) and reduced dust export in negative NAO phases (-4.64 in 2010, -1.97 in 2013), as previously identified in our analysis and former studies using other satellite aerosol dataset over the Mediterranean basin (Moulin et al., 1997; Antoine and Nabileau, 2006; Papadimas et al., 2008).

#### 4 Conclusion

This study provides the first analysis of the spatial and temporal variability of aerosol properties obtained by the daily aerosol retrievals over the western Mediterranean Sea from the POLDER-3/PARASOL spaceborne sensor over its entire period of operation (March 2005 – October 2013). With the exception of two early studies based on METEOSAT (Moulin et al., 1997; 1998) or SeaWiFS (Antoine and Nabileau, 2006), most of the previous efforts dedicated to satellite-derived AOD variability analysis over the Mediterranean basin were based on MODIS data set (Papadimas et al., 2008; Floutsi et al., 2016). On the basis of the quality and robustness of the POLDER-3 ocean operational retrievals over the western Mediterranean (Formenti et al., 2018), we investigated the POLDER-3 AOD due to different aerosol particle size classes (total, fine and coarse components) and particle shapes (coarse spherical and non-spherical contributions) in terms of spatial patterns and temporal variability.

The POLDER-3 aerosol record confirms the high influence of north African desert dust over the region, with a marked maximum in AOD, along with its coarse and coarse non-spherical component in the southernmost part of the region, associated with a decrease in AE, and a seasonal maximum occurring in Spring and Summer. In contrast, the coarse spherical component of AOD remains relatively homogeneously low all year long over the region (AOD<sub>cs</sub> < 0.05). The POLDER-3 retrievals of the fine component of AOD show less spatial variability compared to that observed for the coarse fraction, although AOD<sub>f</sub> tend to be larger in the eastern part of our region of study. Seasonal averages reveal difference by a factor of 2, with minimum AOD<sub>f</sub> of 0.02 (in winter in the south part of the region) and maximum of 0.04 (in spring in the north part of the region) at 865 nm (corresponding respectively to 0.06 and 0.12 for AOD<sub>f</sub> at 550 nm). POLDER-3 also detects a persistent area of relatively high loads of fine particles in the northern part of the Adriatic Sea, characterized by seasonal averages of AOD<sub>f</sub> larger than 0.12 at 550 nm.

At three sites representative of different typical aerosol conditions over the western Mediterranean Sea (namely Ersa, Barcelona, and Lampedusa), POLDER-3 retrievals at 865 nm indicate averages contributions to total AOD at 865 nm ranging between 19 and 20% for coarse spherical particles, 26 and 36% for fine particles (maximum at Ersa), and 44 and 55% for coarse non-spherical particles (maximum at Lampedusa). At Lampedusa, POLDER-3 daily observations record the occurrence of intense or extreme aerosol events (AOD > 1 up to 4.7) consistently with the higher and more direct influence of severe desert dust episodes at this southernmost site. At these three sites, daily POLDER-3 AOD<sub>865 nm</sub> values above 0.3 are associated with low AE and FMF fraction (mean values below 0.5 and 21%, respectively), as well as a dominance of the non-spherical particle fraction in the coarse mode (mean values above 71%), typical of the desert dust influence. The background “clean” conditions associated to very low aerosol loads (POLDER-3 daily AOD<sub>865 nm</sub> values below 0.05) occur 22% of the time around Ersa, 20% around Barcelona and 9.5% around Lampedusa over the POLDER-3 period (2005-2013), highlighting the scarcity of pristine days in this region, especially in its southern part.



Interannual evolutions of March to October POLDER-3-derived AOD, AOD<sub>F</sub> and AOD<sub>C</sub> reveal negative trends over the period 2005-2013, these trends being more pronounced for AOD, and above all AOD<sub>F</sub>, than for the AOD<sub>C</sub> component. Further analysis suggests a link between winter NAO Index and frequency of desert dust episodes (AOD<sub>C</sub> at 865 nm greater than 0.10, f<sub>D</sub>), especially significant in the central part of the western Mediterranean Sea. The analysis of the evolution of clean conditions considering both coarse and fine aerosol components recorded by POLDER-3 over the period March 2005 – October 2013 highlights significant positive trends for clean conditions in terms of fine particles (between +2 and +4% per year) over the region, whereas no tendency is evident for the year-to-year evolution of clean conditions for coarse particles. It is noticeable that the annual frequency of occurrence of clean conditions relative to fine particles reaches values above 75-80% in Erse and Barcelona in the last part of the POLDER-3 operation time, i.e. over the years 2010-2013. These values are much above those retrieved in the beginning of POLDER-3 record (< 57% in Barcelona and < 67% in Erse) over the years 2005-2007. Thus, POLDER-3 aerosol dataset analysis strongly suggests a significant improvement in air quality for the fine mode aerosol component over the western Mediterranean region, consistent with decreasing anthropogenic emissions and surface PM<sub>2.5</sub> reported in Europe around the same period. The occurrence of clean conditions in terms of coarse aerosol component, with no significant detected tendency, is overall less frequent over our region of study, with annual values generally below 50-60%, highlighting the large regional influence of desert dust transported from north African sources.

In conclusion, the high-resolved long-time series POLDER-3 data set of AOD of different size classes provides new and independent insights complementing previous climatology analysis and trend, which, to date, are largely based on the MODIS long-term satellite dataset (e.g. Papadimas et al., 2008; Floutsis et al., 2016). The integration of the POLDER-3 dataset should be most useful as a complement to climate regional models aerosol analysis (Nabat et al., 2013; 2020) for better constraining the evolution and impacts of the variety of aerosols present in the Mediterranean atmosphere.

In addition, based on the series of POLDER missions, the capability of multi-spectral, multi-directional and multi-polarization observations, associated with new inversion schemes, to retrieve aerosol optical and microphysical properties has been successfully proved (Dubovik et al., 2019). Growing attention to polarization observations has resulted in the 3MI instrument that enhances the POLDER concept with more spectral information and a better spatial resolution (Fougnie et al., 2018).

#### Data availability

POLDER-3 data extraction was performed with the program PARASOLASCI (http://www-loa.univ-lille1.fr/~ducous/public/parasolascii/). This version is made available from the AERIS Data and Service Center (http://www.icare.univ-lille1.fr/parasol). Technical details are described at http://www.icare.univ-lille1.fr/projects\_data/parasol/docs/Parasol\_Level-2\_format\_latest.pdf. The definition of the flag index is detailed at page 18 (parameter: quality of the fit).

#### Competing interests

FD is guest editor for the ACP Special Issue of the Chemistry and Aerosols Mediterranean Experiment (ChArMEx) (ACP/AMT inter-journal SI)". The remaining authors declare that they have no conflict of interest.

#### Special issue statement





570 This article is part of the special issue of the Chemistry and Aerosols Mediterranean Experiment (ChArMEx)  
 571 (ACP/AMT inter-journal SI)”. It is not associated with a conference.

## 572 Acknowledgements

573 This work is part of the ChArMEx project supported by CNRS-INSU, ADEME, Météo-France and CEA in the  
 574 framework of the multidisciplinary program MISTRALS (Mediterranean Integrated Studies at Regional And  
 575 Local Scales; <http://mistrals-home.org/>). It has also been supported by the French National Research Agency  
 576 (ANR) through the ADRIMED project (contract ANR-11-BS56-0006) and by the French National Program of  
 577 Spatial Teledetection (PNTS, <http://www.insu.cnrs.fr/pnts>, project n°PNTS-2015-03). L. Mbemba Kabuiku was  
 578 granted by the French Environment and Energy Management Agency (ADEME) and National Center of Space  
 579 Studies (CNES). The French national center for Atmospheric data and services AERIS provided access to the  
 580 POLDER-3 data used.

581 LOA participates in the CaPPA (Chemical and Physical Properties of the Atmosphere) project funded by the  
 582 French National Research Agency (ANR) through the PIA (Programme d'Investissement d'Avenir) under contract  
 583 ANR-11-LABX-0005-01, the Regional Council “Hauts-de-France” and the European Regional Development  
 584 Fund (ERDF). We would like to thank Marc Mallet and Pierre Nabat (CNRM-Toulouse, France) for fruitful  
 585 discussions about the results of this paper.

586

## 587 References

- 588 Ancellet, G., Pelon, J., Totems, J., Chazette, P., Bazureau, A., Sicard, M., Di Iorio, T., Dulac, F., and Mallet, M.:  
 589 Long-range transport and mixing of aerosol sources during the 2013 North American biomass burning episode:  
 590 analysis of multiple lidar observations in the western Mediterranean basin, *Atmos. Chem. Phys.*, 16, 4725-4742,  
 591 <https://doi.org/10.5194/acp-16-4725-2016>, 2016.
- 592 Antoine, D., and Nobileau, D.: Recent increase of Saharan dust transport over the Mediterranean Sea, as revealed  
 593 from ocean color satellite (SeaWiFS) observations, *J. Geophys. Res. Atmos.*, 111, 1–19,  
 594 <https://doi.org/10.1029/2005JD006795>, 2006.
- 595 Barnaba, F., and Gobbi, G. P.: Aerosol seasonal variability over the Mediterranean region and relative impact of  
 596 maritime, continental and Saharan dust particles over the basin from MODIS data in the year 2001, *Atmos. Chem.*  
 597 *Phys.*, 4, 2367–2391, <https://doi.org/10.5194/acp-4-2367-2004>, 2004.
- 598 Boucher, O.: *Atmospheric Aerosols - Properties and Climate Impacts*, 311 pp., Springer,  
 599 <https://doi.org/10.1007/978-94-017-9649-1>, 2015.
- 600 Bréon, F. M., Vermeulen, A., and Descloitres, J.: An evaluation of satellite aerosol products against sunphotometer  
 601 measurements, *Remote Sens. Environ.*, 115, 3102–3111, <https://doi.org/10.1016/j.rse.2011.06.017>, 2011.
- 602 Chazette, P., Totems, J., Ancellet, G., Pelon, J., and Sicard, M.: Temporal consistency of lidar observables during  
 603 aerosol transport events in the framework of the ChArMEx/ADRI MED campaign at Menorca Island in June 2013,  
 604 *Atmos. Chem. Phys.*, 16, 2863–2875, <https://doi.org/10.5194/acp-16-2863-2016>, 2016.
- 605 Chazette, P., Totems, J., and Shang, X.: Transport of aerosols over the French Riviera - link between ground-based  
 606 lidar and spaceborne observations, *Atmos. Chem. Phys.*, 19, 3885-3904, [https://doi.org/10.5194/acp-19-3885-](https://doi.org/10.5194/acp-19-3885-2019)  
 607 [2019](https://doi.org/10.5194/acp-19-3885-2019), 2019.



- 608 Chrit, M., Sartelet, K., Sciare, J., Pey, J., Nicolas, J. B., Marchand, N., Freney, E., Sellegri, K., Beekmann, M.,  
 609 and Dulac, F.: Aerosol sources in the western Mediterranean during summertime: A model-based approach, *Atmos.*  
 610 *Chem. Phys.*, 18, 9631–9659, <https://doi.org/10.5194/acp-18-9631-2018>, 2018.
- 611 Claeys, M., Roberts, G., Mallet, M., Arndt, J., Sellegri, K., Sciare, J., Wenger, J., and Sauvage, B.: Optical,  
 612 physical and chemical properties of aerosols transported to a coastal site in the western Mediterranean: a focus on  
 613 primary marine aerosols, *Atmos. Chem. Phys.*, 17, 7891–7915, <https://doi.org/10.5194/acp-17-7891-2017>, 2017.
- 614 Cusack, M., Alastuey, A., Pérez, N., Pey, J., and Querol, X.: Trends of particulate matter (PM<sub>2.5</sub>) and chemical  
 615 composition at a regional background site in the Western Mediterranean over the last nine years (2002–2010),  
 616 *Atmos. Chem. Phys.*, 12, 8341–8357, <https://doi.org/10.5194/acp-12-8341-2012>, 2012.
- 617 Denjean, C., Cassola, F., Mazzino, A., Triquet, S., Chevaillier, S., Grand, N., Bourriane, T., Momboisse, G.,  
 618 Sellegri, K., Schwarzenbock, A., Freney, E., Mallet, M., and Formenti, P.: Size distribution and optical properties  
 619 of mineral dust aerosols transported in the western Mediterranean. *Atmos. Chem. Phys.*, 16, 1081–1104,  
 620 <https://doi.org/10.5194/acp-16-1081-2016>, 2016.
- 621 Di Biagio, C., Doppler, L., Gaimoz, C., Grand, N., Ancellet, G., Raut, J.-C., Beekmann, M., Borbon, A., Sartelet,  
 622 K., Attié, J.-L., Ravetta, F., and Formenti, P.: Continental pollution in the western Mediterranean basin: vertical  
 623 profiles of aerosol and trace gases measured over the sea during TRAQA 2012 and SAFMED 2013, *Atmos. Chem.*  
 624 *Phys.*, 15, 9611–9630, <https://doi.org/10.5194/acp-15-9611-2015>, 2015.
- 625 Di Biagio, C., Formenti, P., Doppler, L., Gaimoz, C., Grand, N., Ancellet, G., Attié, J.-L., Bucci, S., Dubuisson,  
 626 P., Fierli, F., Mallet, M., and Ravetta, F.: Continental pollution in the Western Mediterranean basin: large  
 627 variability of the aerosol single scattering albedo and influence on the direct shortwave radiative effect, *Atmos.*  
 628 *Chem. Phys.*, 16, 10591–10607, <https://doi.org/10.5194/acp-16-10591-2016>, 2016.
- 629 Drugé, T., Nabat, P., Mallet, M., and Somot, S.: Model simulation of ammonium and nitrate aerosols distribution  
 630 in the Euro-Mediterranean region and their radiative and climatic effects over 1979–2016, *Atmos. Chem. Phys.*,  
 631 19, 3707–3731, <https://doi.org/10.5194/acp-19-3707-2019>, 2019.
- 632 Dubovik, O., Li, Z., Mishchenko, M. I., Tanré, D., Karol, Y., Bojkov, B., Cairns, B., Diner, D. J., Espinosa, W.  
 633 R., Goloub, P., Gu, X., Hasekamp, O., Hong, J., Hou, W., Knobelspiesse, K. D., Landgraf, J., Li, L., Litvinov, P.,  
 634 Liu, Y., Lopatin, A., Marbach, T., Maring, H., Martins, V., Meijer, Y., Milinevsky, G., Mukai, S., Parol, F., Qiao,  
 635 Y., Remer, L., Rietjens, J., Sano, I., Stammes, P., Stammes, S., Sun, X., Tabary, P., Travis, L. D., Waquet, F., Xu,  
 636 F., Yan, C. and Yin, D.: Polarimetric remote sensing of atmospheric aerosols: Instruments, methodologies, results,  
 637 and perspectives, *J. Quant. Spectrosc. Radiat. Transf.*, 224, 474–511, doi:10.1016/J.JQSRT.2018.11.024, 2019.
- 638 Dubovik, O., Sinyuk, A., Lapyonok, T., Holben, B. N., Mishchenko, M., Yang, P., Eck, T. F., Volten, H., Muñoz,  
 639 O., Veihelmann, B., van der Zande, W. J., Leon, J.-F., Sorokin, M., and Slutsker, I.: Application of spheroid  
 640 models to account for aerosol particle nonsphericity in remote sensing of desert dust, *J. Geophys. Res.*, 111,  
 641 D11208, <https://doi.org/10.1029/2005JD006619>, 2006.
- 642 Dulac, F., Tanré, D., Bergametti, G., Buat-Ménard, P., Desbois, M., and Sutton, D.: Assessment of the African  
 643 airborne dust mass over the western Mediterranean Sea using Meteosat data, *J. Geophys. Res.*, 97, 2489–2506,  
 644 <https://doi.org/10.1029/91JD02427>, 1992.
- 645 Floutsis, A.A., M.B. Korras-Carraca, C. Matsoukas, N. Hatzianastassiou, and G. Biskos, Climatology and trends  
 646 of aerosol optical depth over the Mediterranean basin during the last 12 years (2002–2014) based on Collection



- 647 006 MODIS-Aqua data, *Sci. Total Environ.*, 551–552, 292–293, <https://doi.org/10.1016/j.scitotenv.2016.01.192>,  
 648 2016.
- 649 Formenti, P. (Coord.), *Mediterranean aerosol properties, Part VII in: Mediterranean Atmospheric Chemistry in the*  
 650 *Mediterranean – Vol. 2, From Pollutant Sources to Impacts*, Dulac, F., Sauvage, S., and Eric Hamonou (Eds.),  
 651 Springer, in prep., 2020.
- 652 Formenti, P., Mbemba Kabuiku, L., Chiapello, I., Ducos, F., Dulac, F., and Tanré, D.: Aerosol optical properties  
 653 derived from POLDER-3/PARASOL (2005–2013) over the western Mediterranean Sea – Part 1: Quality  
 654 assessment with AERONET and in situ airborne observations, *Atmos. Meas. Tech.*, 11, 6761–6784,  
 655 <https://doi.org/10.5194/amt-11-6761-2018>, 2018.
- 656 Fougnie, B., Improvement of the PARASOL Radiometric In-Flight Calibration Based on Synergy Between  
 657 Various Methods Using Natural Targets, in *IEEE Transactions on Geoscience and Remote Sensing*, vol. 54, no.  
 658 4, pp. 2140–2152, April 2016, doi: 10.1109/TGRS.2015.2496322, 2016.
- 659 Fougnie, B., Marbach, T., Lacan, A., Lang, R., Schlüssel, P., Poli, G., Munro, R. and Couto, A. B.: The multi-  
 660 viewing multi-channel multi-polarisation imager – Overview of the 3MI polarimetric mission for aerosol and cloud  
 661 characterization, *J. Quant. Spectrosc. Radiat. Transf.*, 219, 23–32, doi:10.1016/j.jqsrt.2018.07.008, 2018.
- 662 Georgoulas, A. K., Alexandri, G., Kourtidis, K. A., Lelieveld, J., Zanis, P., Pöschl, U., Levy, R., Amiridis, V.,  
 663 Marinou, E., and Tsikerdekis, A.: Spatiotemporal variability and contribution of different aerosol types to the  
 664 aerosol optical depth over the Eastern Mediterranean, *Atmos. Chem. Phys.*, 16, 13853–13884,  
 665 <https://doi.org/10.5194/acp-16-13853-2016>, 2016.
- 666 Gkikas, A., Basart, S., Hatzianastassiou, N., Marinou, E., Amiridis, V., Kazadzis, S., Pey, J., Querol, X., Jorba,  
 667 O., Gassó, S., and Baldasano, J. M.: Mediterranean intense desert dust outbreaks and their vertical structure based  
 668 on remote sensing data, *Atmos. Chem. Phys.*, 16, 8609–8642, <https://doi.org/10.5194/acp-16-8609-2016>, 2016.
- 669 Gkikas, A., Hatzianastassiou, N., Mihalopoulos, N., Katsoulis, V., Kazadzis, S., Pey, J., Querol, X., and Torres,  
 670 O.: The regime of intense desert dust episodes in the Mediterranean based on contemporary satellite observations  
 671 and ground measurements, *Atmos. Chem. Phys.*, 13, 12135–12154, <https://doi.org/10.5194/acp-13-12135-2013>,  
 672 2013.
- 673 Hatzianastassiou, N., A. Gkikas, N. Mihalopoulos, O. Torres, and B. D. Katsoulis (2009), Natural versus  
 674 anthropogenic aerosols in the eastern Mediterranean basin derived from multiyear TOMS and MODIS satellite  
 675 data, *J. Geophys. Res.*, 114, D24202, <https://doi.org/10.1029/2009JD011982>.
- 676 Herman, M., Deuzé, J. L., Marchand, A., Roger, B., and Lallart, P.: Aerosol remote sensing from  
 677 POLDER/ADEOS over the ocean: Improved retrieval using a nonspherical particle model, *J. Geophys. Res.*, 110,  
 678 D10S02, <https://doi.org/10.1029/2004JD004798>, 2005.
- 679 Holben, B. N., Tanré, D., Smirnov, A., Eck, T. F., Slutsker, I., Abuhassan, N., Newcomb, W. W., Schafer, J. S.,  
 680 Chatenet, B., Lavenue, F., Kaufman, Y. J., Castle, J. Vande, Setzer, A., Markham, B., Clark, D., Frouin, R.,  
 681 Halthore, R., Karneli, A., O'Neill, N. T., Pietras, C., Pinker, R. T., Voss, K., and Zibordi, G.: An emerging ground-  
 682 based aerosol climatology: Aerosol optical depth from AERONET, *J. Geophys. Res. Atmos.*, 106, 12067–12097,  
 683 <https://doi.org/10.1029/2001JD900014>, 2001.
- 684 Hurrell, J. W., Decadal trend in the North Atlantic Oscillation: Regional temperatures and precipitations, *Science*,  
 685 269, 676–679, <https://doi.org/10.1126/science.269.5224.676>, 1995.



686 Kaskaoutis D. G., Shailesh Kumar Kharol, N. Sifakis, P.T. Nastos, Anu Rani Sharma, K.V.S. Badarinath, H.D.  
 687 Kambezidis, Satellite monitoring of the biomass-burning aerosols during the wildfires of August 2007 in Greece:  
 688 Climate implications, Atmospheric Environment, Volume 45, Issue 3, Pages 716-726,  
 689 <https://doi.org/10.1016/j.atmosenv.2010.09.043>, 2011.  
 690 Laj, P., Klausen, J., Bilde, M., Plass-Duelmer, C., Pappalardo, G., Clerbaux, C., Baltensperger, U., Hjorth, J.,  
 691 Simpson, D., Reimann, S. and Coheur, P. F.: Measuring atmospheric composition change, Atmos. Environ., 43,  
 692 5351–5414, <https://doi.org/10.1016/j.atmosenv.2009.08.020>, 2009.  
 693 Laj, P., Bigi, A., Rose, C., Andrews, E., Lund Myhre, C., Collaud Coen, M., Lin, Y., Wiedensohler, A., Schulz,  
 694 M., Ogren, J. A., Fiebig, M., Gliß, J., Mortier, A., Pandolfi, M., Petäja, T., Kim, S.-W., Aas, W., Putaud, J.-P.,  
 695 Mayol-Bracero, O., Keywood, M., Labrador, L., Aalto, P., Ahlberg, E., Alados Arboledas, L., Alastuey, A.,  
 696 Andrade, M., Artiñano, B., Ausmeel, S., Arsov, T., Asmi, E., Backman, J., Baltensperger, U., Bastian, S., Bath,  
 697 O., Beukes, J. P., Brem, B. T., Bukowiecki, N., Conil, S., Couret, C., Day, D., Dayanlis, W., Degorska, A.,  
 698 Eleftheriadis, K., Fetzis, P., Favez, O., Flentje, H., Gini, M. I., Gregorič, A., Gysel-Beer, M., Hallar, A. G.,  
 699 Hand, J., Hoffer, A., Hueglin, C., Hooda, R. K., Hyvärinen, A., Kalapov, I., Kalivitis, N., Kasper-Giebl, A., Kim,  
 700 J. E., Kouvarakis, G., Kranjc, I., Krejci, R., Kulmala, M., Labuschagne, C., Lee, H.-J., Lihavainen, H., Lin, N.-H.,  
 701 Löschau, G., Luoma, K., Marinoni, A., Martins Dos Santos, S., Meinhardt, F., Merkel, M., Metzger, J.-M.,  
 702 Mihalopoulos, N., Nguyen, N. A., Ondracek, J., Pérez, N., Perrone, M. R., Petit, J.-E., Picard, D., Pichon, J.-M.,  
 703 Pont, V., Prats, N., Prenni, A., Reisen, F., Romano, S., Sellegri, K., Sharma, S., Schauer, G., Sheridan, P., Sherman,  
 704 J. P., Schütze, M., Schwerin, A., Sohmer, R., Sorribas, M., Steinbacher, M., Sun, J., Titos, G., Toczko, B., Tuch,  
 705 T., Tulet, P., Tunved, P., Vakkari, V., Velarde, F., Velasquez, P., Villani, P., Vratolis, S., Wang, S.-H., Weinhold,  
 706 K., Weller, R., Yela, M., Yus-Diez, J., Zdimal, V., Zieger, P., and Zikova, N.: A global analysis of climate-relevant  
 707 aerosol properties retrieved from the network of Global Atmosphere Watch (GAW) near-surface observatories,  
 708 Atmos. Meas. Tech., 13, 4353–4392, <https://doi.org/10.5194/amt-13-4353-2020>, 2020.  
 709 Lelieveld, J., Berresheim, H., Borrmann, S., Crutzen, P. J., Dentener, F. J., Fischer, H., Feichter, J., Flatau, P. J.,  
 710 Heland, J., Holzinger, R., Korrmann, R., Lawrence, M. G., Levin, Z., Markowicz, K. M., Mihalopoulos, N.,  
 711 Minikin, a, Ramanathan, V., De Reus, M., Roelofs, G. J., Scheeren, H. a, Sciare, J., Schlager, H., Schultz, M.,  
 712 Siegmund, P., Steil, B., Stephanou, E. G., Stier, P., Traub, M., Warneke, C., Williams, J., and Ziereis, H.: Global  
 713 air pollution crossroads over the Mediterranean, Science, 298, 794–9, <https://doi.org/10.1126/science.1075457>,  
 714 2002.  
 715 Lyamani, H., Valenzuela, A., Perez-Ramirez, D., Toledano, C., Granados-Muñoz, M. J., Olmo, F. J., and Alados-  
 716 Arboledas, L.: Aerosol properties over the western Mediterranean basin: temporal and spatial variability, Atmos.  
 717 Chem. Phys., 15, 2473–2486, <https://doi.org/10.5194/acp-15-2473-2015>, 2015.  
 718 Mallet, M., Dulac, F., Formenti, P., Nabat, P., Sciare, J., Roberts, G., Pelon, J., Ancellet, G., Tanré, D., Parol, F.,  
 719 Denjean, C., Brogniez, G., di Sarra, A., Alados-Arboledas, L., Arndt, J., Auriol, F., Blarel, L., Bourrienne, T.,  
 720 Chazette, P., Chevaillier, S., Claeys, M., D'Anna, B., Derimian, Y., Desboeufs, K., Di Iorio, T., Doussin, J.-F.,  
 721 Durand, P., Féron, A., Freney, E., Gaimoz, C., Goloub, P., Gómez-Amo, J. L., Granados-Muñoz, M. J., Grand,  
 722 N., Hamonou, E., Jankowiak, I., Jeannot, M., Léon, J.-F., Maillé, M., Mailler, S., Meloni, D., Menut, L.,  
 723 Momboisse, G., Nicolas, J., Podvin, T., Pont, V., Rea, G., Renard, J.-B., Roblou, L., Schepanski, K.,  
 724 Schwarzenboeck, A., Sellegri, K., Sicard, M., Solmon, F., Somot, S., Torres, B., Totems, J., Triquet, S., Verdier,  
 725 N., Verwaerde, C., Waquet, F., Wenger, J., and Zapf, P.: Overview of the Chemistry-Aerosol Mediterranean



- 726 Experiment/Aerosol Direct Radiative Forcing on the Mediterranean Climate (ChArMEx/ADRIMED) summer  
 727 2013 campaign, *Atmos. Chem. Phys.*, 16, 455–504, <https://doi.org/10.5194/acp-16-455-2016>, 2016.
- 728 Menut, L., Siour, G., Mailler, S., Couvidat, F., and Bessagnet, B.: Observations and regional modeling of aerosol  
 729 optical properties, speciation and size distribution over northern Africa and western Europe, *Atmos. Chem. Phys.*,  
 730 16, 12961–12982, <https://doi.org/10.5194/acp-16-12961-2016>, 2016.
- 731 Michoud, V., Sciare, J., Sauvage, S., Dusanter, S., Léonardis, T., Gros, V., Kalogridis, C., Zannoni, N., Féron, A.,  
 732 Petit, J.-E., Crenn, V., Baisnée, D., Sarda-Estève, R., Bonnaire, N., Marchand, N., DeWitt, H. L., Pey, J., Colomb,  
 733 A., Gheusi, F., Szidat, S., Stavroulas, I., Borbon, A., and Locoge, N.: Organic carbon at a remote site of the western  
 734 Mediterranean Basin: composition, sources and chemistry during the ChArMEx SOP2 field experiment, *Atmos.*  
 735 *Chem. Phys.*, 17, 8837–8865, <https://doi.org/10.5194/acp-17-8837-2017>, 2017.
- 736 Moulin, C., Lambert, C. E., Dayan, U., Masson, V., Ramonet, M., Bousquet, P., Legrand, M., Balkanski, Y. J.,  
 737 Guelle, W., Marticorena, B., Bergametti, G., and Dulac, F.: Satellite climatology of African dust transport in the  
 738 Mediterranean atmosphere, *J. Geophys. Res.*, 103, 13137, doi:10.1029/98JD00171, 1998.
- 739 Moulin, C., Lambert, C. E., Dulac, F., and Dayan, U.: Control of atmospheric export of dust from North Africa by  
 740 the North Atlantic Oscillation, *Nature*, 387, 691–694, <https://doi.org/10.1038/42679>, 1997.
- 741 Nabat, P., Somot, S., Cassou, C., Mallet, M., Michou, M., Bouniol, D., Decharme, B., Drugé, T., Roehrig, R., and  
 742 Saint-Martin, D.: Modulation of radiative aerosols effects by atmospheric circulation over the Euro-Mediterranean  
 743 region, *Atmos. Chem. Phys.*, 20, 8315–8349, <https://doi.org/10.5194/acp-20-8315-2020>, 2020.
- 744 Nabat, P., Somot, S., Mallet, M., Chiapello, I., Morcrette, J. J., Solmon, F., Szopa, S., Dulac, F., Collins, W., Ghan,  
 745 S., Horowitz, L. W., Lamarque, J. F., Lee, Y. H., Naik, V., Nagashima, T., Shindell, D., and Skeie, R.: A 4-D  
 746 climatology (1979–2009) of the monthly tropospheric aerosol optical depth distribution over the Mediterranean  
 747 region from a comparative evaluation and blending of remote sensing and model products, *Atmos. Meas. Tech.*,  
 748 6, 1287–1314, doi:10.5194/amt-6-1287-2013, 2013.
- 749 Pandolfi, M., Alastuey, A., Pérez, N., Reche, C., Castro, I., Shatalov, V., and Querol, X.: Trends analysis of PM  
 750 source contributions and chemical tracers in NE Spain during 2004–2014: a multi-exponential approach, *Atmos.*  
 751 *Chem. Phys.*, 16, 11787–11805, <https://doi.org/10.5194/acp-16-11787-2016>, 2016.
- 752 Pandolfi, M., Alados-Arboledas, L., Alastuey, A., Andrade, M., Angelov, C., Artiñano, B., Backman, J.,  
 753 Baltensperger, U., Bonasoni, P., Bukowiecki, N., Collaud Coen, M., Conil, S., Coz, E., Crenn, V., Dudoitis, V.,  
 754 Ealo, M., Eleftheriadis, K., Favez, O., Fetfatzis, P., Fiebig, M., Flentje, H., Ginot, P., Gysel, M., Henzing, B.,  
 755 Hoffer, A., Holubova Smejkalova, A., Kalapov, I., Kalivitis, N., Kouvarakis, G., Kristensson, A., Kulmala, M.,  
 756 Lihavainen, H., Lunder, C., Luoma, K., Lyamani, H., Marinoni, A., Mihalopoulos, N., Moerman, M., Nicolas, J.,  
 757 O'Dowd, C., Petäjä, T., Petit, J.-E., Pichon, J. M., Prokopciuk, N., Putaud, J.-P., Rodríguez, S., Sciare, J., Sellegri,  
 758 K., Swietlicki, E., Titos, G., Tuch, T., Tunved, P., Ulevicius, V., Vaishya, A., Vana, M., Virkkula, A., Vratolis,  
 759 S., Weingartner, E., Wiedensohler, A., and Laj, P.: A European aerosol phenomenology – 6: scattering properties  
 760 of atmospheric aerosol particles from 28 ACTRIS sites, *Atmos. Chem. Phys.*, 18, 7877–7911,  
 761 <https://doi.org/10.5194/acp-18-7877-2018>, 2018.
- 762 Papadimas, C. D., Hatzianastassiou, N., Mihalopoulos, N., Querol, X., and Vardavas, I.: Spatial and temporal  
 763 variability in aerosol properties over the Mediterranean basin based on 6- year (2000–2006) MODIS data: *J.*  
 764 *Geophys. Res.*, 113, D11205, <https://doi.org/10.1029/2007JD009189>, 2008.
- 765 Rea, G., Turquety, S., Menut, L., Briant, R., Mailler, S., and Siour, G.: Source contributions to 2012 summertime



766 aerosols in the Euro-Mediterranean region, *Atmos. Chem. Phys.*, 15, 8013–8036, doi:10.5194/acp-15-8013-2015,  
 767 2015.

768 Remer, L.R., R. C. Levy, S. Mattoo, D. Tanré, P. Gupta, Y. Shi, V. Sawyer, L. A. Munchak, Y. Zhou, M. Kim, C.  
 769 Ichoku, F. Patadia, R.-R. Li, S. Gassó, R. G. Kleidman, and B. N. Holben, The Dark Target Algorithm for  
 770 Observing the Global Aerosol System: Past, Present, and Future, *Remote Sens.* 2020, 12, 2900 ;  
 771 doi :10.3390/rs12182900,2020.

772 Ricaud, P., Zbinden, R., Catoire, V., Brocchi, V., Dulac, F., Hamonou, E., Canonici, J.-C., El Amraoui, L.,  
 773 Massart, S., Pignatelli, B., Dayan, U., Nabat, P., Sciare, J., Ramonet, M., Delmotte, M., di Sarra, A., Sferlazzo, D.,  
 774 di Iorio, T., Piacentini, S., Cristofanelli, P., Mihalopoulos, N., Kouvarakis, G., Pikridas, M., Savvides, C.,  
 775 Mamouri, R.-E., Nisantzi, A., Hadjimitsis, D., Attié, J.-L., Ferré, H., Kangah, Y., Jaidan, N., Guth, J., Jacquet, P.,  
 776 Chevrier, S., Robert, C., Bourdon, A., Bourdinot, J.-F., Etienne, J.-C., Krysztofak, G., and Théron, P.: The GLAM  
 777 airborne campaign across the Mediterranean basin, *Bull. Am. Met. Soc.*, 99, 361–380,  
 778 <https://doi.org/10.1175/BAMS-D-16-0226.1>, 2018.

779 Salvador, P., Alonso-Pérez, S., Pey, J., Artíñano, B., de Bustos, J. J., Alastuey, A., and Querol, X.: African dust  
 780 outbreaks over the western Mediterranean Basin: 11-year characterization of atmospheric circulation patterns and  
 781 dust source areas, *Atmos. Chem. Phys.*, 14, 6759–6775, <https://doi.org/10.5194/acp-14-6759-2014>, 2014.

782 Shaheen, A., Wu, R., Aldabash, M., Long-term AOD trend assessment over the Eastern Mediterranean region: A  
 783 comparative study including a new merged aerosol product, *Atmosph. Environ.*, 238, 117736,  
 784 <https://doi.org/10.1016/j.atmosenv.2020.117736>, 2020.

785 Sič, B., El Amraoui, L., Piacentini, A., Marécal, V., Emili, E., Cariolle, D., Prather, M., and Attié, J.-L.: Aerosol  
 786 data assimilation in the chemical-transport model MOCAGE during the TRAQA/ChArME campaign: Aerosol  
 787 optical depth, *Atmos. Meas. Tech.*, 9, 5535–5554, <https://doi.org/10.5194/amt-9-5535-2016>, 2016.

788 Sicard, M., R. Barragan, F. Dulac, L. Alados-Arboledas, and M. Mallet : Aerosol optical, microphysical and  
 789 radiative properties at regional background insular sites in the western Mediterranean, *Atmos. Chem. Phys.*, 16,  
 790 12177–12203, <https://doi.org/10.5194/acp-16-12177-2016>, 2016.

791 Tanré, D., Bréon, F. M., Deuzé, J. L., Dubovik, O., Ducos, F., François, P., Goloub, P., Herman, M., Lifermann,  
 792 A. and Waquet, F.: Remote sensing of aerosols by using polarized, directional and spectral measurements within  
 793 the A-Train: the PARASOL mission, *Atmos. Meas. Tech.*, 4, 1383–1395, [https://doi.org/10.5194/amt-4-1383-](https://doi.org/10.5194/amt-4-1383-2011)  
 794 [2011](https://doi.org/10.5194/amt-4-1383-2011), 2011.

795

796

797

798

799

800

801

802

803

804

805

806

807





808  
 809

	AOD			AE			AOD <sub>F</sub>			AOD <sub>C</sub>		
	North	Central	South	North	Central	South	North	Central	South	North	Central	South
Winter (DJF)	0.062	0.064	0.074	0.950	0.792	0.723	0.025	0.022	0.021	0.037	0.042	0.058
Spring (MAM)	0.106	0.115	0.155	1.064	0.855	0.724	0.043	0.038	0.040	0.063	0.078	0.115
Summer (JJA)	0.106	0.126	0.153	0.947	0.819	0.737	0.038	0.038	0.040	0.068	0.088	0.113
Fall (SON)	0.079	0.086	0.104	0.963	0.831	0.734	0.033	0.030	0.031	0.047	0.057	0.074
<b>Annual</b>	<b>0.090</b>	<b>0.099</b>	<b>0.124</b>	<b>0.985</b>	<b>0.826</b>	<b>0.729</b>	<b>0.035</b>	<b>0.032</b>	<b>0.033</b>	<b>0.055</b>	<b>0.067</b>	<b>0.091</b>
	Fine Mode Fraction %			AOD <sub>CNS</sub>			AOD <sub>CS</sub>					
	North	Central	South	North	Central	South	North	Central	South			
Winter (DJF)	40	34	30	0.033	0.034	0.048	0.013	0.016	0.018			
Spring (MAM)	42	34	29	0.048	0.062	0.088	0.021	0.026	0.029			
Summer (JJA)	36	31	27	0.046	0.058	0.091	0.021	0.027	0.031			
Fall (SON)	40	35	30	0.041	0.047	0.059	0.015	0.019	0.023			
<b>Annual</b>	<b>40</b>	<b>33</b>	<b>29</b>	<b>0.043</b>	<b>0.051</b>	<b>0.073</b>	<b>0.018</b>	<b>0.022</b>	<b>0.026</b>			

810  
 811  
 812  
 813  
 814

**Table 1a.** The 8 (winter) or 9-year (March 2005 – October 2013) climatological seasonal averaged values of POLDER-3 advanced aerosol products at 865 nm for the north (NW MED), central (CW MED), and south (SW MED) parts of western Mediterranean basins (defined in Figure 2). Maximum values are reported in red, minimum, in blue.

	AOD			AOD <sub>F</sub>			AOD <sub>C</sub>			Fine Mode Fraction %		
	North	Central	South	North	Central	South	North	Central	South	North	Central	South
Winter (DJF)	0.099	0.093	0.106	0.069	0.059	0.058	0.030	0.035	0.049	65	60	56
Spring (MAM)	0.168	0.166	0.204	0.118	0.104	0.109	0.049	0.062	0.095	70	62	57
Summer (JJA)	0.163	0.180	0.208	0.110	0.110	0.117	0.053	0.070	0.091	66	61	57
Fall (SON)	0.126	0.128	0.144	0.089	0.082	0.084	0.037	0.046	0.060	66	61	57
<b>Annual</b>	<b>0.141</b>	<b>0.143</b>	<b>0.167</b>	<b>0.098</b>	<b>0.089</b>	<b>0.093</b>	<b>0.043</b>	<b>0.053</b>	<b>0.074</b>	<b>67</b>	<b>61</b>	<b>57</b>

815  
 816  
 817  
 818  
 819  
 820  
 821  
 822  
 823  
 824  
 825  
 826  
 827  
 828  
 829  
 830  
 831  
 832  
 833  
 834  
 835  
 836  
 837  
 838  
 839  
 840  
 841  
 842  
 843  
 844

**Table 1b.** Same as Table 1a for AOD, AOD<sub>F</sub>, AOD<sub>C</sub>, and Fine Mode Fraction at 550 nm for the north (NW MED), central (CW MED), and south (SW MED) parts of western Mediterranean basins (defined in Figure 2). Maximum values are reported in red, minimum, in blue.



845  
 846  
 847

	Ersa N <sub>ACSP</sub> = 1242 - N <sub>BVC</sub> = 556		Barcelona N <sub>ACSP</sub> = 1241 - N <sub>BVC</sub> = 540		Lampedusa N <sub>ACSP</sub> = 1320 - N <sub>BVC</sub> = 612	
	Mean ± SD	Range Min – Max	Mean ± SD	Range Min – Max	Mean ± SD	Range Min – Max
ACSP AOD <sub>865 nm</sub>	0.09 ± 0.07	0.01 – 0.68	0.10 ± 0.04	0.01 – 1.05	0.15 ± 0.18	0.02 – 4.72
ACSP AOD <sub>F 865 nm</sub>	0.03 ± 0.03	<0.01 – 0.16	0.04 ± 0.03	<0.01 – 0.19	0.04 ± 0.03	<0.01 – 0.35
ACSP AOD <sub>C 865 nm</sub>	0.06 ± 0.06	<0.01 – 0.65	0.07 ± 0.07	<0.01 – 0.94	0.11 ± 0.16	<0.01 – 4.37
ACSP AE <sub>865-670</sub>	0.94 ± 0.53	0.01 – 2.23	0.90 ± 0.50	-0.07 – 2.33	0.67 ± 0.42	0.00 – 2.24
ACSP FMF (%)	38 ± 23	3 – 100	37 ± 22	1 – 97	28 ± 18	3 – 100
BVC AOD <sub>CNS 865nm</sub>	0.04 ± 0.04	<0.01 – 0.48	0.05 ± 0.05	<0.01 – 0.42	0.08 ± 0.09	<0.01 – 1.00
BVC AOD <sub>CS 865nm</sub>	0.02 ± 0.03	<0.01 – 0.24	0.02 ± 0.03	<0.01 – 0.34	0.03 ± 0.03	<0.01 – 0.33

848  
 849  
 850  
 851  
 852  
 853  
 854  
 855  
 856  
 857  
 858  
 859  
 860  
 861  
 862  
 863  
 864  
 865  
 866  
 867  
 868  
 869  
 870  
 871  
 872  
 873  
 874  
 875  
 876  
 877  
 878  
 879  
 880  
 881

**Table 2.** Statistics of POLDER-3 daily retrievals of AOD, AOD<sub>F</sub>, AOD<sub>C</sub>, AE, FMF (Fine Mode Fraction), AOD<sub>CS</sub>, and AOD<sub>CNS</sub> at three main stations, Ersa, Barcelona, and Lampedusa for the period March 2005 - October 2013. The numbers of POLDER-3 retrievals available at each station for all clear sky pixels (ACSP) and for best viewing conditions (BVC) are reported.



882  
 883  
 884  
 885  
 886  
 887  
 888

Trend per year Region	AOD 865 nm		AOD <sub>COARSE</sub> 865 nm		AOD <sub>FINE</sub> 865 nm	
	Annual means	Monthly anomalies	Annual means	Monthly anomalies	Annual means	Monthly anomalies
NW MED	<b>- 0.0030 ± 0.0011*</b>	<b>- 0.0031 ± 0.0006**</b>	- 0.0010 ± 0.0009	<b>- 0.0012 ± 0.0005*</b>	<b>- 0.0020 ± 0.0005**</b>	<b>- 0.0019 ± 0.0003**</b>
CW MED	<b>- 0.0035 ± 0.0010*</b>	<b>- 0.0035 ± 0.0007**</b>	- 0.0015 ± 0.0009	<b>- 0.0016 ± 0.0006**</b>	<b>- 0.0020 ± 0.0004**</b>	<b>- 0.0019 ± 0.0003**</b>
SW MED	- 0.0037 ± 0.0019	<b>- 0.0043 ± 0.0012**</b>	- 0.0021 ± 0.0016	<b>- 0.0027 ± 0.0010*</b>	<b>- 0.0016 ± 0.0004**</b>	<b>- 0.0016 ± 0.0003**</b>

889  
 890  
 891  
 892  
 893  
 894  
 895  
 896

**Table 3.** POLDER-3 865 nm AOD, AOD<sub>COARSE</sub> and AOD<sub>FINE</sub> trends per year derived from March-October annual means and monthly mean anomalies over the 2005-2013 period for NW MED, CW MED, SW MED. The corresponding annual evolutions are shown in Figure 8. Trends (year<sup>-1</sup>) are shown with their standard deviations ( $\pm 1\sigma$ ). Values in bold indicate statistically significant trends at \* 95% confidence level and \*\* 99% confidence level, as determined by the Student t-test.

Trend per year Station	AOD 865 nm		AOD <sub>COARSE</sub> 865 nm		AOD <sub>FINE</sub> 865 nm	
	Annual means	Monthly anomalies	Annual means	Monthly anomalies	Annual means	Monthly anomalies
Ersa	<b>- 0.0035 ± 0.0014*</b>	<b>- 0.0030 ± 0.0008**</b>	- 0.0012 ± 0.0012	- 0.0011 ± 0.0008	<b>- 0.0024 ± 0.0004**</b>	<b>- 0.0019 ± 0.0003**</b>
Barcelona	<b>- 0.0050 ± 0.0021*</b>	<b>- 0.0046 ± 0.0011**</b>	- 0.0021 ± 0.0017	<b>- 0.0020 ± 0.0009*</b>	<b>- 0.0029 ± 0.0005**</b>	<b>- 0.0026 ± 0.0004**</b>
Lampedusa	- 0.0037 ± 0.0028	- 0.0025 ± 0.0018	- 0.0021 ± 0.0026	- 0.0009 ± 0.0016	<b>- 0.0017 ± 0.0003**</b>	<b>- 0.0015 ± 0.0004**</b>

897  
 898  
 899  
 900  
 901  
 902  
 903  
 904  
 905  
 906  
 907  
 908

**Table 4.** POLDER-3 865 nm AOD, AOD<sub>COARSE</sub> and AOD<sub>FINE</sub> trends per year derived from March-October annual means and monthly mean anomalies over the 2005-2013 period for Ersa, Barcelona, and Lampedusa. The corresponding annual evolutions are shown in Figure 9. Trends (year<sup>-1</sup>) are shown with their standard deviations ( $\pm 1\sigma$ ). Values in bold indicate statistically significant trends at \* 95% confidence level and \*\* 99% confidence level, as determined by the Student t-test.

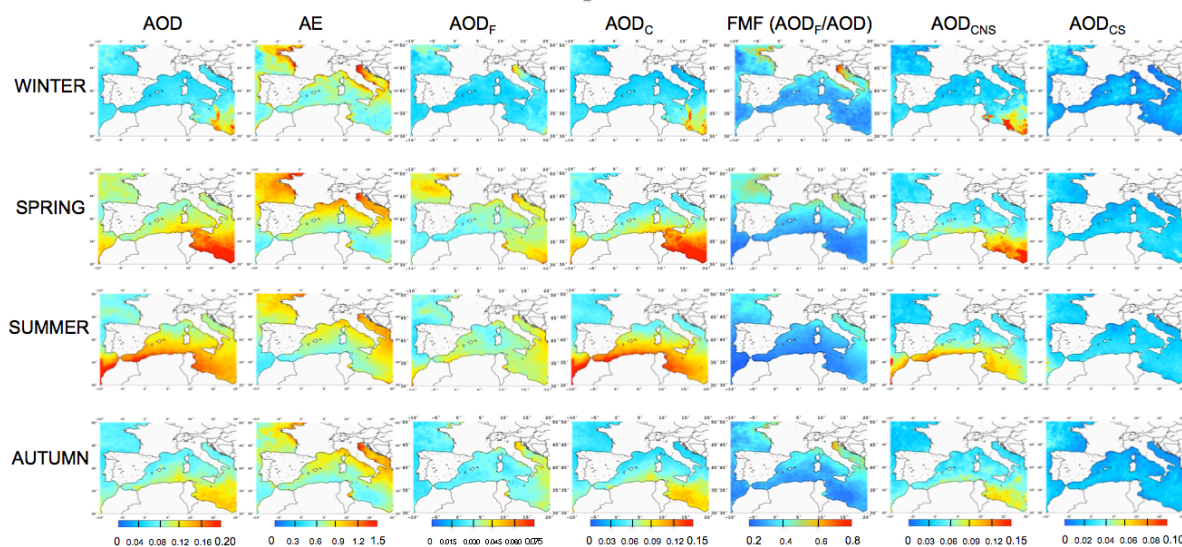


**Figure 1.** Climatological seasonal maps for AOD, AE, AOD<sub>F</sub>, AOD<sub>C</sub>, FMF (Fine Mode Fraction derived from AOD<sub>F</sub>/AOD), AOD<sub>CNS</sub>, and AOD<sub>CS</sub> retrieved by POLDER-3 at 865 nm over the period March 2005–October 2013. Seasons are ordered from the top to the bottom : Winter is December–January–February, Spring March–April–May, Summer June–July–August, Autumn September–October–November.

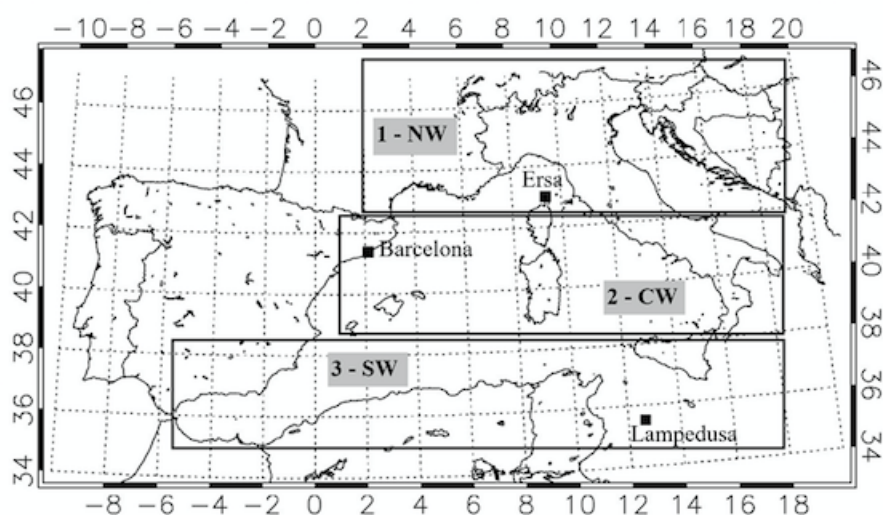


**Figure 2.** Definition of the three geographical sub-regions used to analyze POLDER-3 aerosol retrievals over the area of study: 1. NW Med, 42–46°N, 02°E–20°E – 2. CW MED, 38–42°N, 01°W–20°E, 3. SW MED, 34–38°N, 06°W–20°E. The three sites considered in this study are reported, i.e., Ersat (43.00367°N, 09.35929°E), Barcelona (41.38925°N, 02.11206°E), and Lampedusa (35.51667°N, 12.63167°E).

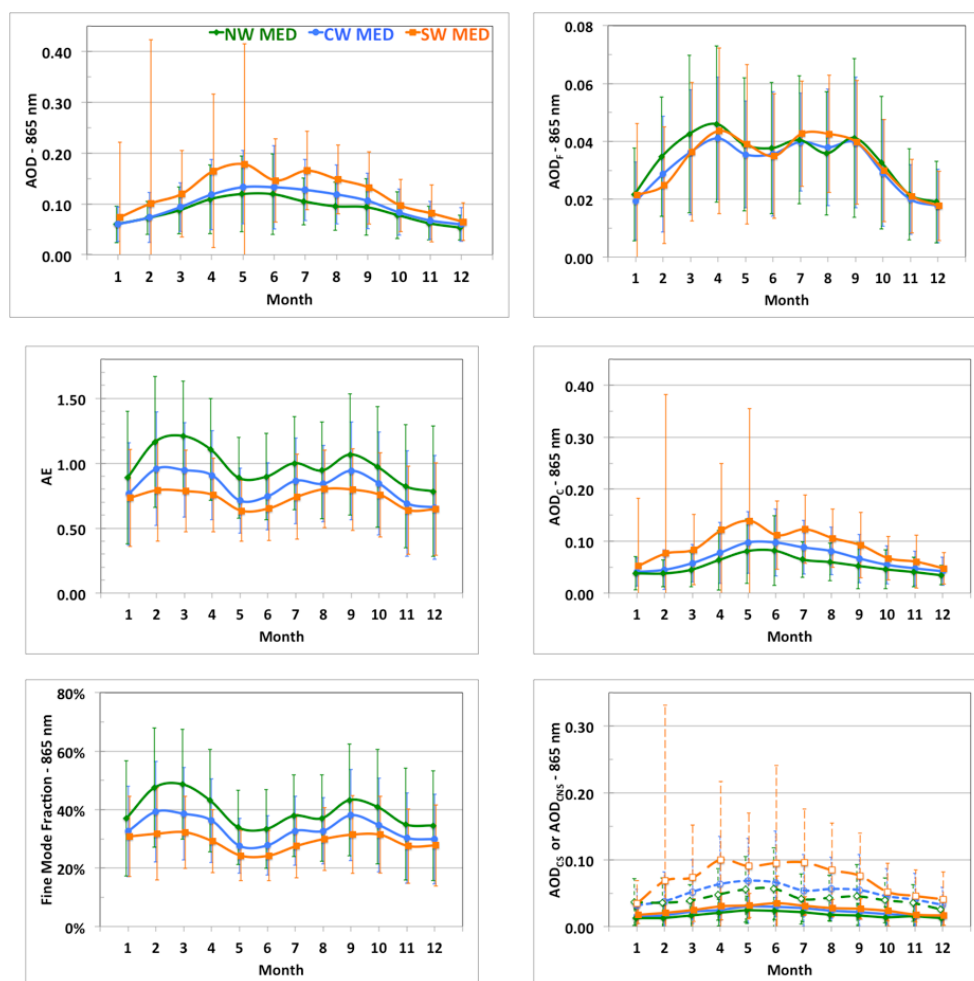


**Figure 3.** The 9-year (March 2005 – October 2013) climatological seasonal cycle of -Left column: AOD (top), Angström Exponent (middle), Fine Mode Fraction (bottom) – Right column: AOD<sub>Fine</sub> (top), AOD<sub>Coarse</sub> (middle), AOD<sub>Coarse Spherical</sub> (continuous lines) and AOD<sub>Coarse Non Spherical</sub> (dashed lines) (bottom), derived from POLDER-3 at 865 nm. The green, blue, orange curves are respectively for the north (NW MED), central (CW MED), and south (SW MED) parts of western Mediterranean basins (defined in Figure 2).



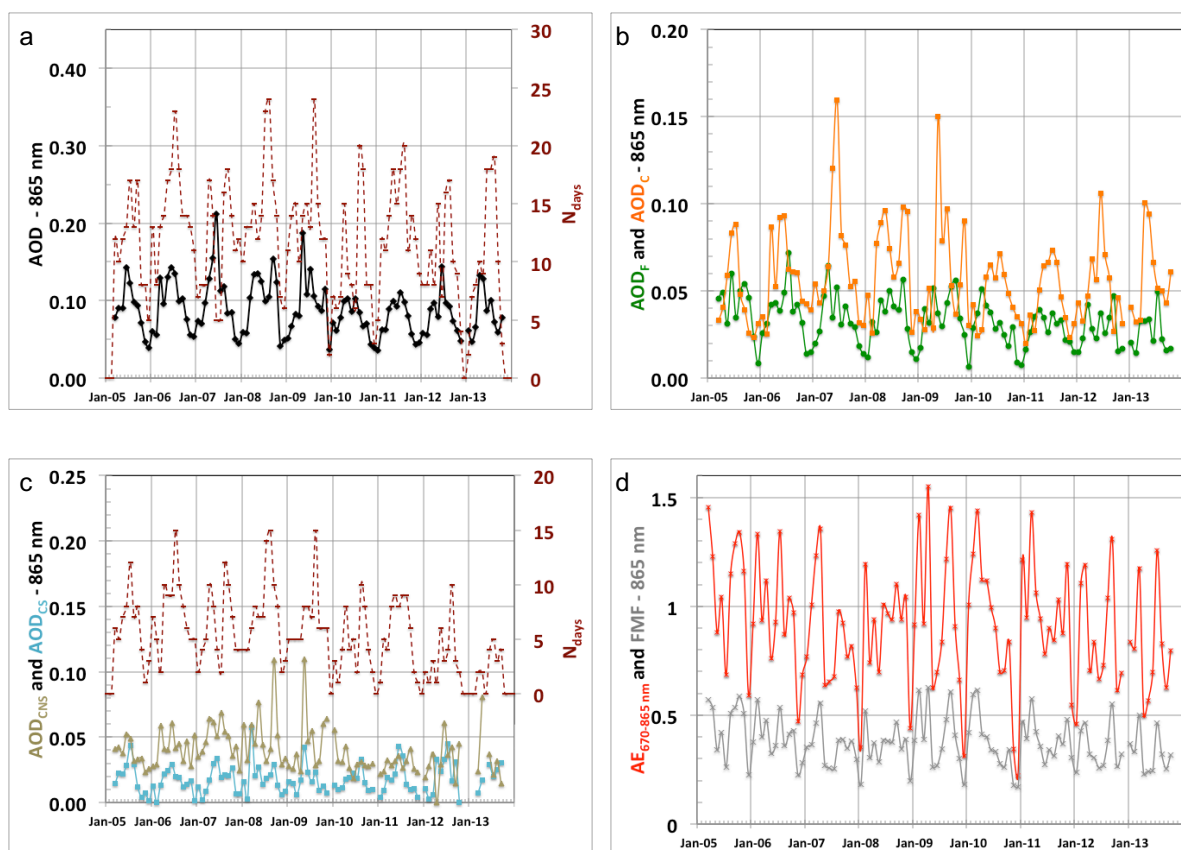


**Figure 4.** POLDER-3 monthly mean retrievals of (a) AOD, (b) AOD<sub>F</sub> and AOD<sub>C</sub>, (c) AOD<sub>CNS</sub> and AOD<sub>CS</sub>, (d) AE<sub>865-670</sub> and FMF at 865 nm at Ersa over the period 2005-2013. The number of days of observations available for each month is reported for all clear days (right axis of Figure 4a), and for best viewing conditions (right axis of Figure 4c) necessary for retrievals of AOD<sub>CNS</sub> and AOD<sub>CS</sub>.

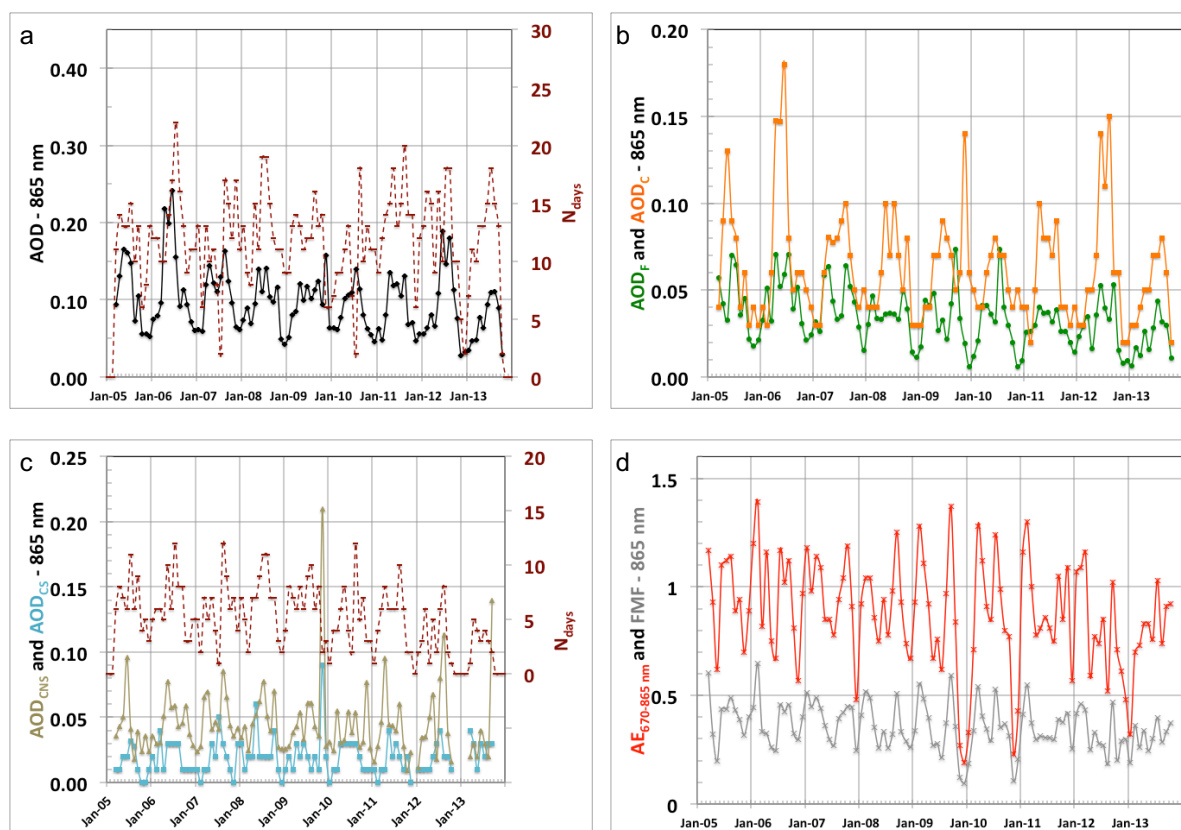
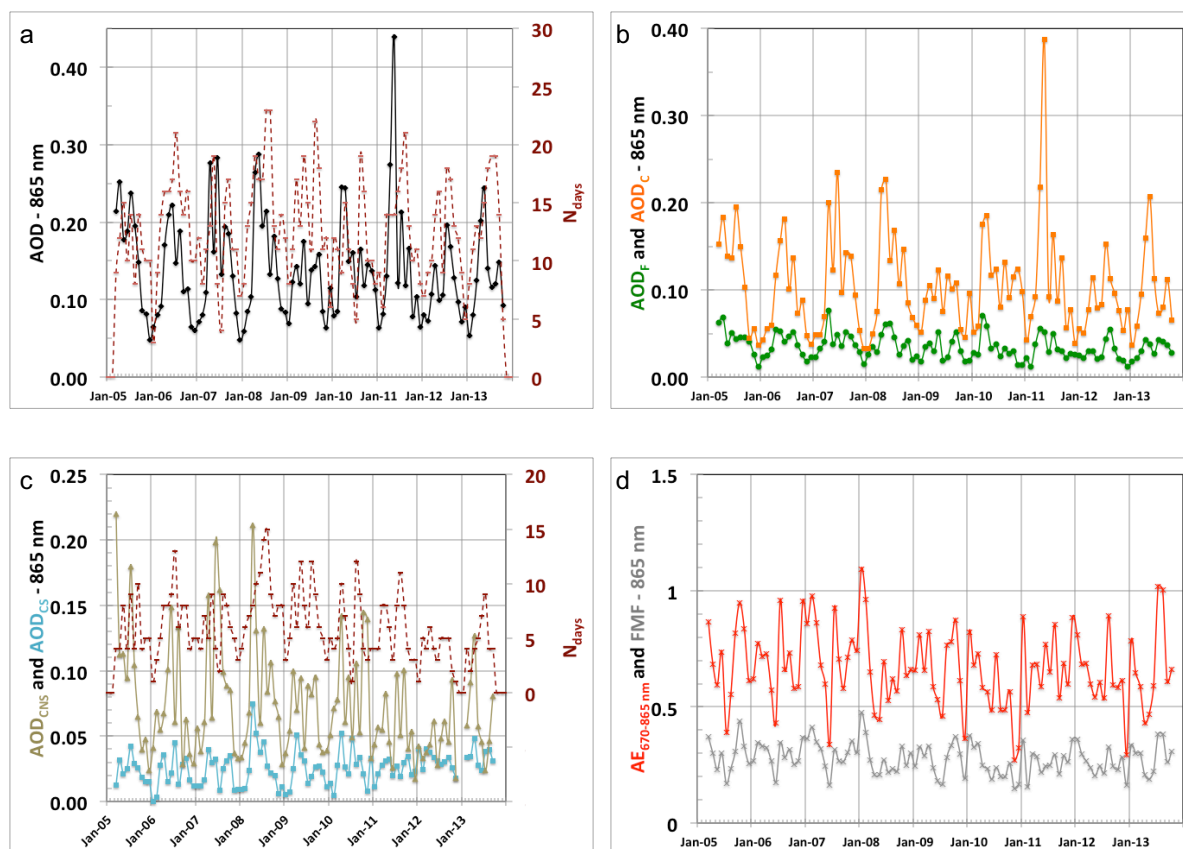
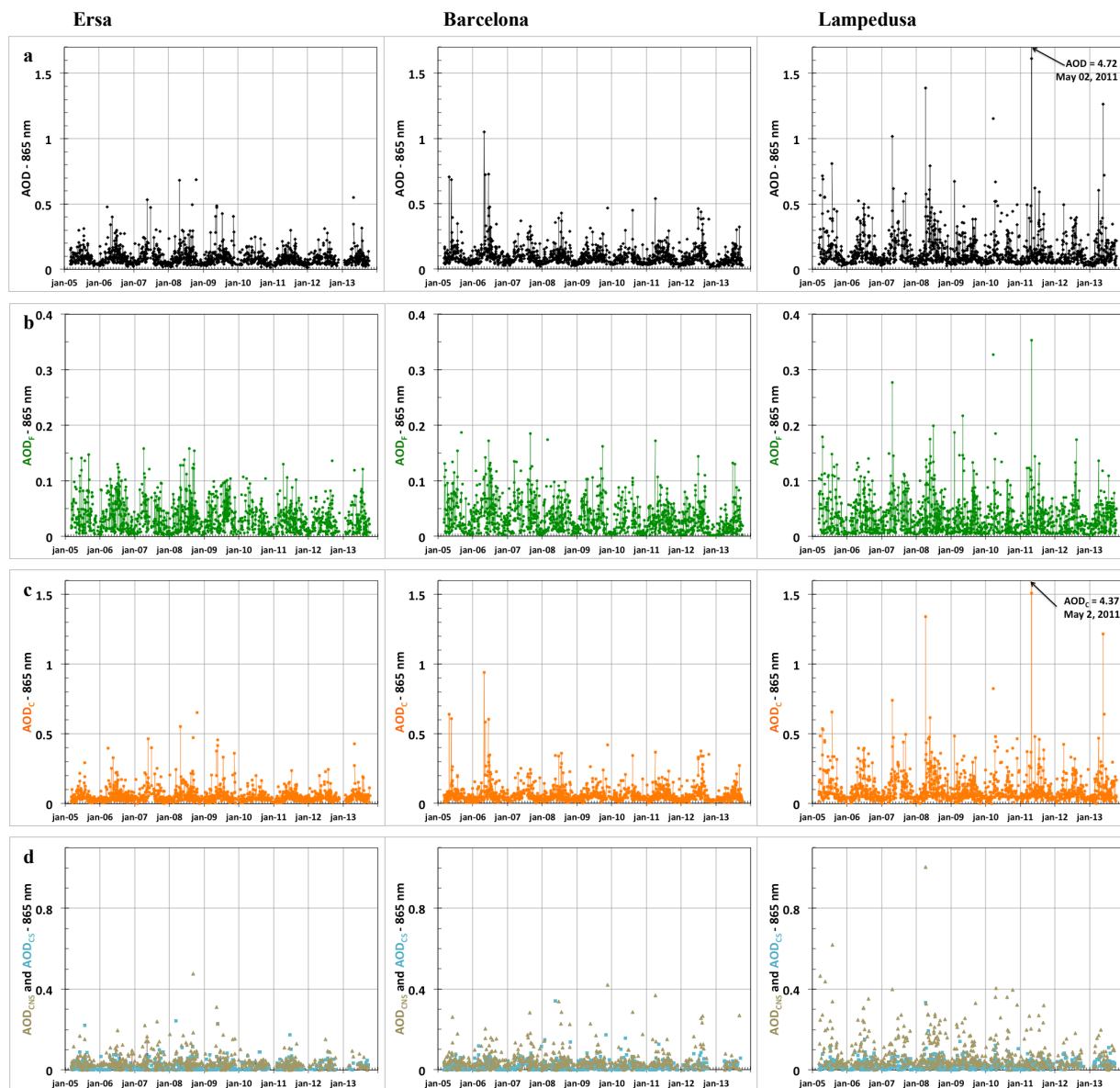


Figure 5. Same as Figure 4 for Barcelona.



**Figure 6.** Same as Figure 4 for Lampedusa. Note that the scale of Figure 6b is different from that of Figure 4b and 5b.



**Figure 7.** POLDER-3 daily retrievals of a- AOD, b- AOD<sub>F</sub>, c- AOD<sub>C</sub>, d- AOD<sub>CNS</sub> and AOD<sub>CS</sub> at 865 nm at Ersaa (left panels), Barcelona (middle panels), and Lampedusa (right panels) over its whole period of operation (March 4, 2005 – October 10, 2013).

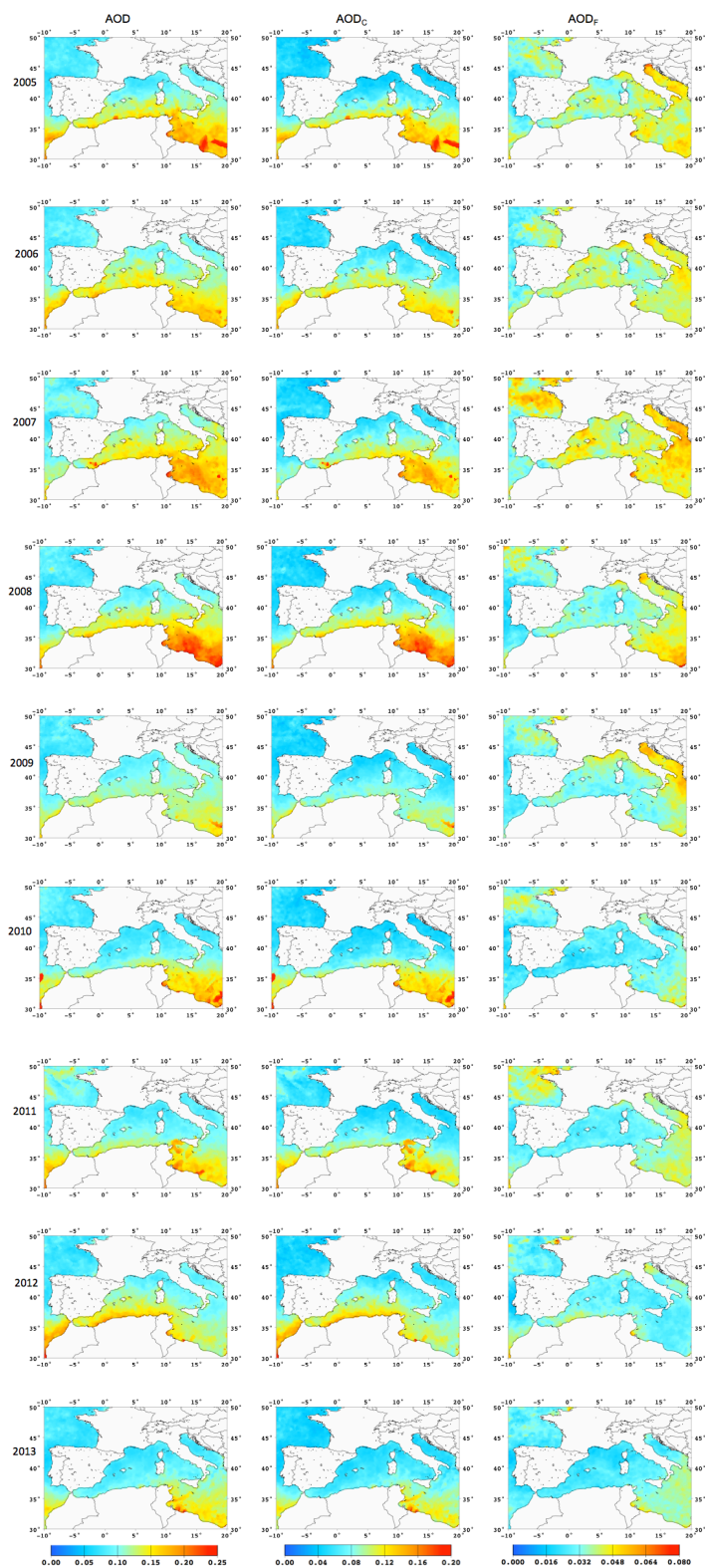


**Figure 8.** March-October annual averages of POLDER-3 AOD (left), AOD<sub>C</sub> (middle), AOD<sub>F</sub> (right) at 865 nm from 2005 to 2013.

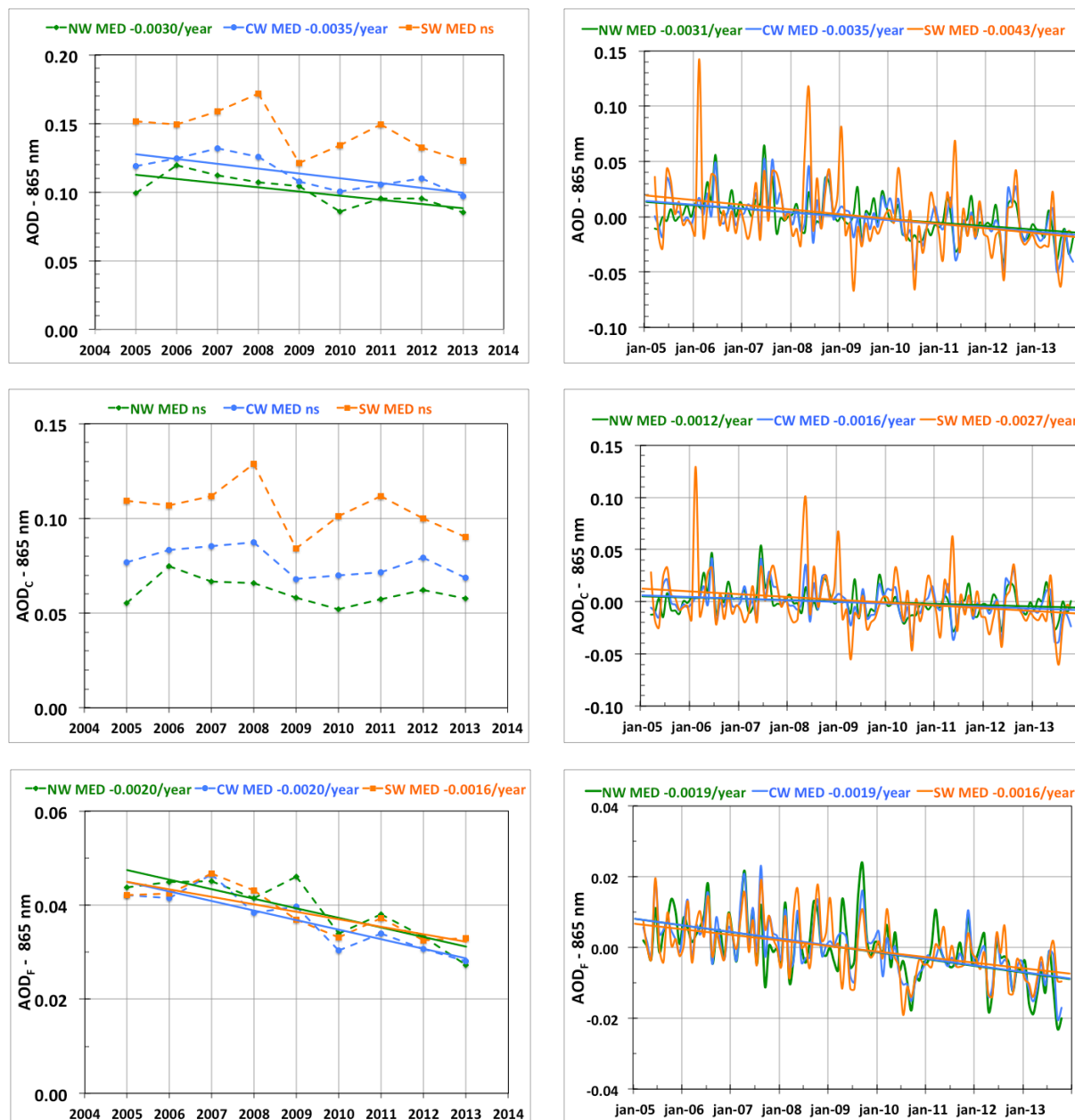


**Figure 9.** March to October yearly means (left column) and monthly anomalies (right column) of POLDER-3 retrievals at 865 nm over the period 2005–2013: AOD (top), AOD<sub>COARSE</sub> (middle), AOD<sub>FINE</sub> (bottom) spatially averaged over north (NW MED, green curves), central (CW MED, blue curves), and south (SW MED, orange curves) parts of western Mediterranean basins (defined Figure 2). Trends (year<sup>-1</sup>) are plotted when significant according to the Student t-test, as summarized in Table 3.



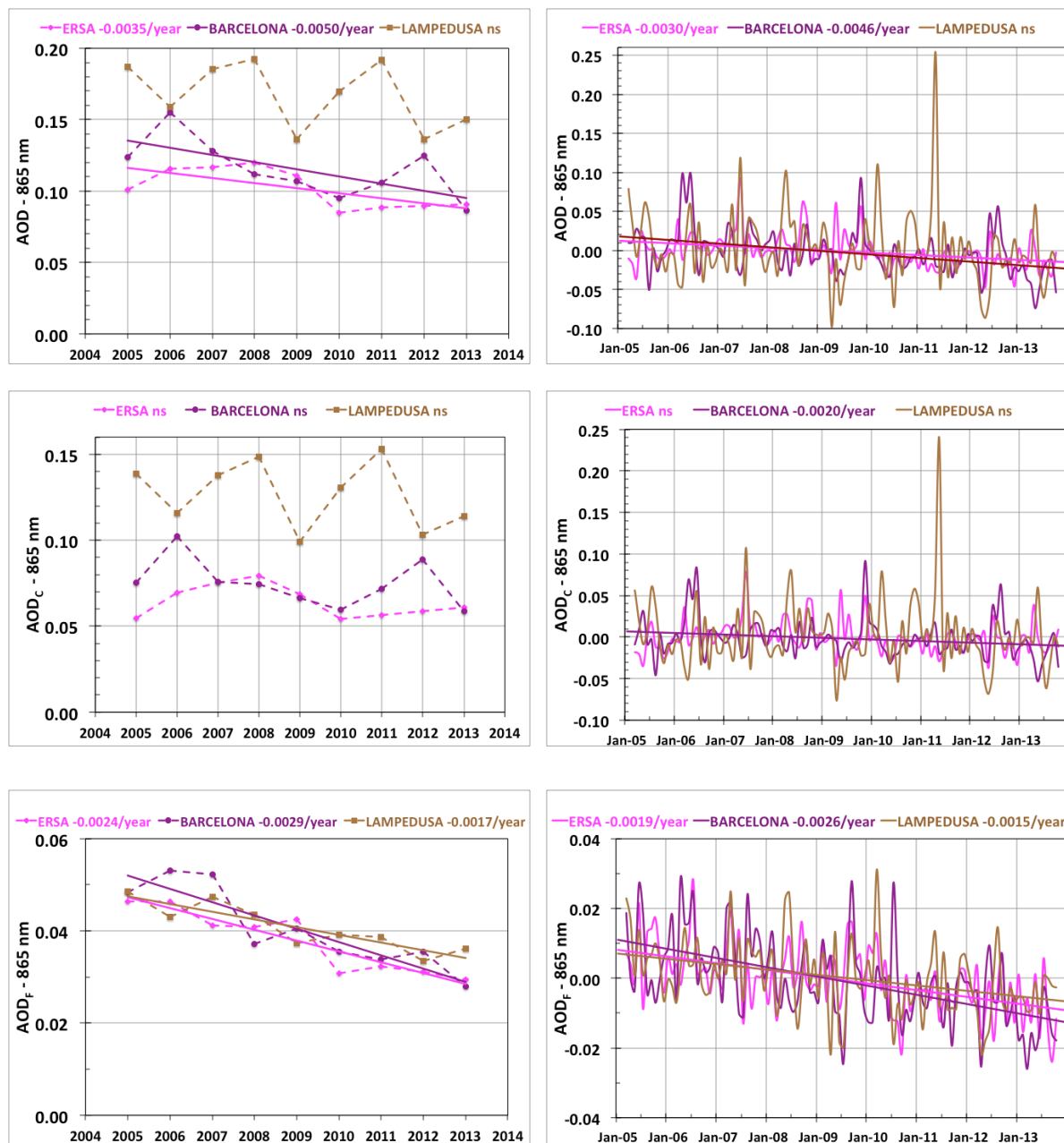


**Figure 10.** March to October yearly means (left column) and monthly anomalies (right column) of POLDER-3 retrievals at 865 nm over the period 2005–2013: AOD (top), AOD<sub>COARSE</sub> (middle), AOD<sub>FINE</sub> (bottom) extracted at Ersa (pink curves), Barcelona (purple curves), and Lampedusa (brown curves). Trends (year<sup>-1</sup>) are plotted when significant according to the Student t-test, as summarized in Table 4.

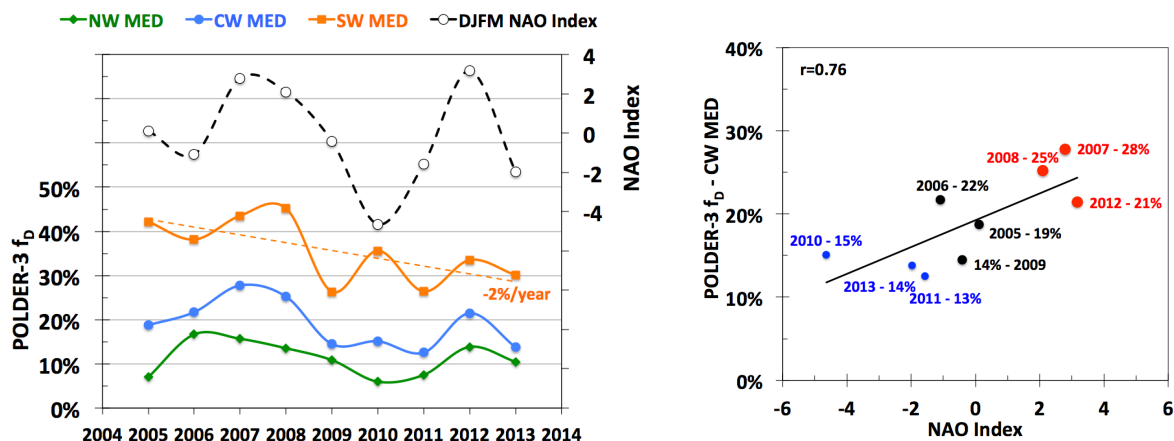


**Figure 11.** Left: Time series of the NAO winter Index (scale on the right axis, open circles) and of the following annual relative frequency ( $f_D$ ) of POLDER-3 AOD<sub>C</sub> at 865 nm  $\geq 0.10$  for the three sub-regions (NW MED in green, CW MED in blue, SW MED in orange) over the period March-2005–October 2013. The only significant trend of  $f_D$ /year is reported on the graph for SW MED. Right: Scatterplot of  $f_D$  versus preceding winter NAO Index for the CW MED region.

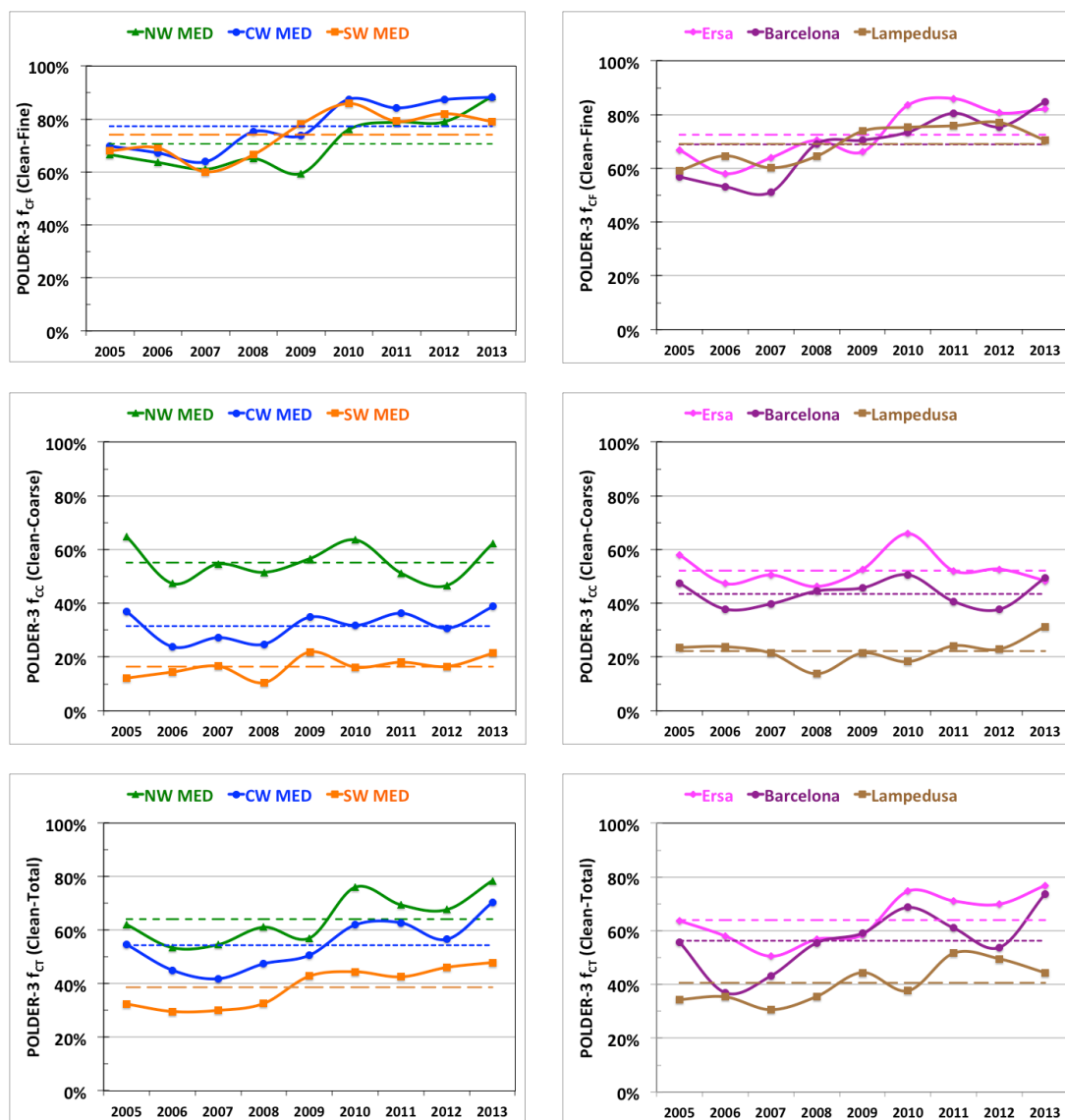


**Figure 12.** Left: Time series of annual (March–October) relative frequencies of occurrence of clean conditions for fine mode aerosol component (POLDER-3  $AOD_F$  865 nm below 0.05,  $f_{CF}$ ; top panel), coarse mode aerosol component (POLDER-3  $AOD_C$  865 nm below 0.05,  $f_{CC}$ ; middle panel), and total aerosol (POLDER-3  $AOD$  865 nm lower or equal to 0.10,  $f_{CT}$ ; bottom panel) over the period 2005–2013 for the three sub-regions NW MED, CW MED, SW MED. The dashed lines indicate the multi-year annual averages of relative frequencies. Right: Same for the three sites of Ersa, Barcelona, and Lampedusa.

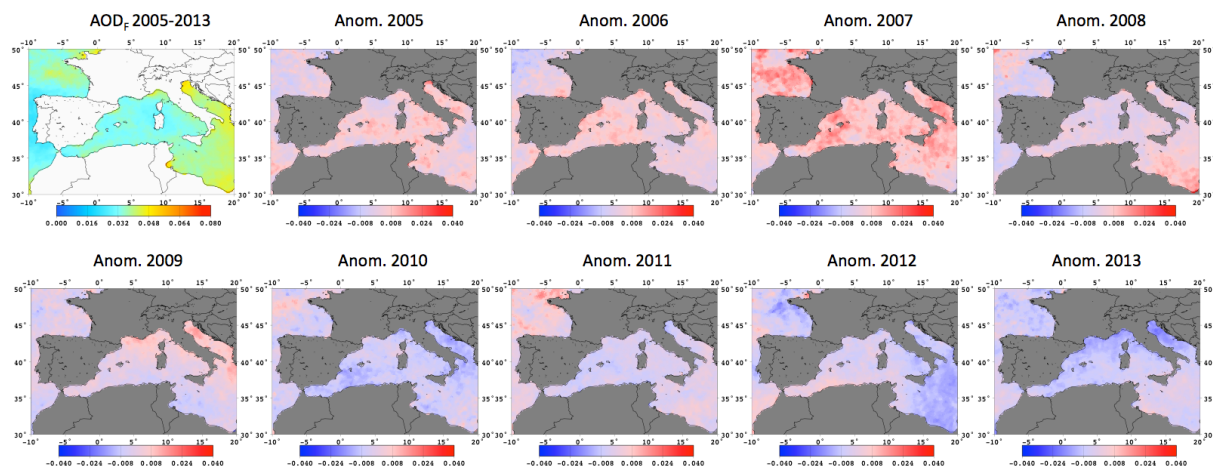


**Figure 13.** POLDER-3 AOD<sub>F</sub> at 865 nm averaged over the March-October period and the 9 years 2005-2013 (top left) and associated AOD<sub>F</sub> anomalies for each year.

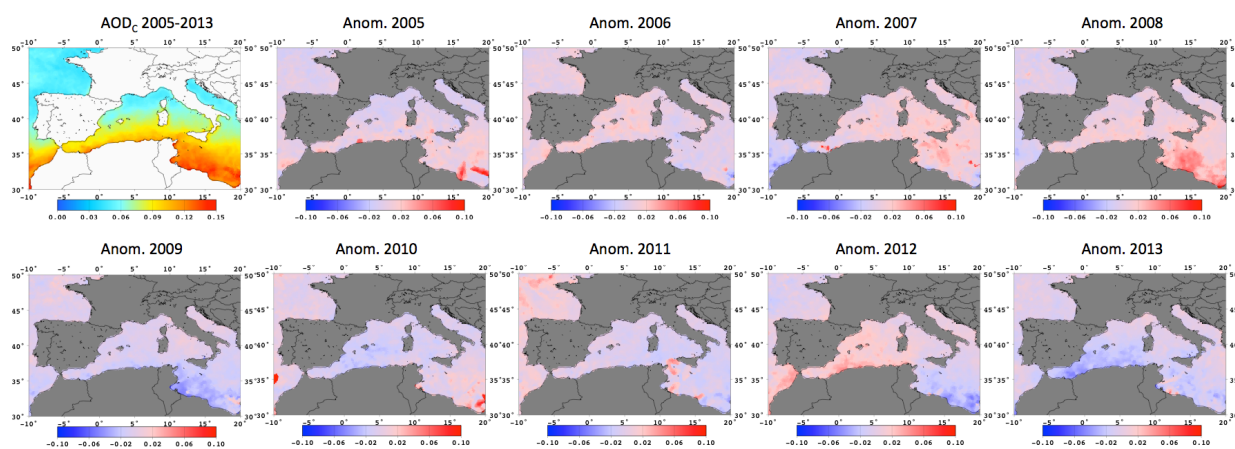


**Figure 14.** POLDER-3 AOD<sub>c</sub> at 865 nm averaged over the March-October period and the 9 years 2005-2013 (top left) and associated AOD<sub>c</sub> anomalies for each year.